A Review of Thermal Transport in Low-Dimensional Materials Under External Perturbation: Effect of Strain, Substrate, and Clustering

Cheng Shao, Xiaoxiang Yu, Nuo Yang, Yanan Yue & Hua Bao

Taylor & Francis
Taylor & Francis Group

A Review of Thermal Transport in Low-Dimensional Materials Under External Perturbation: Effect of Strain, Substrate, and Clustering

Cheng Shao[a], Xiaoxiang Yu[b], Nuo Yang[b], Yanan Yue[c], and Hua Bao[a]

[a]University of Michigan–Shanghai Jiao Tong University Joint Institute, Shanghai Jiao Tong University, Shanghai, P.R. China; [b]State Key Laboratory of Coal Combustion, Huazhong University of Science and Technology, Wuhan, P. R. China, and Nano Interface Center for Energy, School of Energy and Power Engineering, Huazhong University of Science and Technology, Wuhan, P. R. China; [c]School of Power and Mechanical Engineering, Wuhan University, Wuhan, P. R. China

ABSTRACT

Due to their exceptional electrical, thermal, and optical properties, low-dimensional (LD) materials are very promising for many applications, such as nanoelectronic devices, energy storage, energy conversion, and thermal management. The thermal performance of LD materials is often an important consideration in these applications. Although freestanding LD materials exhibit interesting thermal properties, they are almost never used in such a form. Instead, they are often integrated into a certain environment; for example, in a composite material or on a substrate. Due to the large surface-to-volume ratio of LD materials, the environment usually has a strong impact on the thermal transport properties of these materials. The thermal behavior of the LD materials can be completely different from the freestanding form. The effect of environmental perturbation on thermal transport properties has recently attracted a lot of research interest. In this article, we aim to provide a comprehensive review of how the typical external perturbations, including tensile strain, substrate, and clustering, can affect the thermal transport properties of LD materials. Emphasis will be placed on how these perturbations affect the lattice structure, phonon dispersion, lattice anharmonicity, and thermal conductivity. We will also summarize the achievements and the remaining challenges on this research topic.

Introduction

The emergence of low-dimensional materials in the last few decades has attracted enormous research interest in their structures and electronic [1–3], optical [4–6], and thermal properties [7, 8]. For example, carbon nanotubes (CNTs) and graphene are representative one-dimensional (1D) and two-dimensional (2D) materials to investigate the unique electron and phonon transport properties [7, 8]. The extremely high thermal conductivity of CNTs and graphene make them very promising for thermal management applications, including thermal interface materials [9–11], high thermal conductivity composites [12, 13], and interconnects for electronic devices [14]. Some 1D materials, such as polyethylene (PE) chains and nanofibers, are found to have high thermal conductivity, which suggests that polymers can be a cheap alternative to metals for heat dissipation in electronics and optoelectronics [15, 16]. Other 2D materials, such as molybdenum disulfide (MoS_2), silicene, and phosphorene, are regarded as promising candidates for next-generation semiconductor devices [2, 3,

17–19]. The recent successful exfoliation of bismuth telluride (Bi_2Te_3) quintuple layer (QL) makes it very promising in thermoelectric applications [20, 21].

Thermal transport in LD materials is an important factor for most of these applications. For example, in thermal management, it is desirable to achieve high thermal conductivity using LD materials [10, 22]. The thermal transport properties of 2D materials are also an important factor for designing 2D material–based transistors [23, 24]. In thermoelectric applications, low lattice thermal conductivity is desired to achieve good performance [25].

Intrinsic thermal transport properties of LD materials have been studied extensively. There are some reviews about the heat transfer in LD materials; for example, about CNTs [22], graphene [26, 27], or other LD materials [28–30]. The intrinsic thermal conductivities of LD materials can span a few orders of magnitude. For example, extremely high thermal conductivity values have been reported in measurements of carbon-based materials like CNTs [31–33] and graphene [8, 34–36]. There are also claims that CNTs and graphene can have diverged thermal conductivities [37–39]. Some materials like the Bi_2Te_3 quintuple have a thermal conductivity of 1–3 W/mK [20, 21]. The thermal conductivity of LD materials can also be affected or tuned by dimension size [40], doping [41–43], and chemical functionalization [44], and there are a few reviews on these effects [45–47].

On the other hand, the high surface-to-volume ratio feature makes LD materials more sensitive to external environmental perturbations. For example, residual strain is unavoidable in LD materials during the process of fabrication and transfer [48–51]. In real applications, LD materials are usually integrated into a certain environment, such as being supported on a substrate, forming a cluster (e.g., CNT bundle), or being embedded in matrix materials. It is found that the external perturbations have strong impacts on thermal transport properties of LD materials [52–55]. Considerable studies have been carried out in the past a few years on this topic, resulting in some intriguing and sometimes controversial findings. For example, tensile strain generally leads to reduction in thermal conductivity of bulk materials [56], but its effect on graphene and other LD materials remains a matter of debate [38, 57–60]. Supporting on a substrate will usually induce additional phonon scattering and thus lower the thermal conductivity [36, 61–63], but some studies reported an enhancement in thermal conductivity when supported on a particular substrate [64]. Forming a cluster is believed to be unfavorable to thermal transport [65, 66], but some simulations and experimental results have shown that the interlayer coupling could facilitate the thermal transport in certain situations [67, 68]. In different studies, researchers used different approaches and considered different types of external perturbations. It seems that different simulations or experimental methods used to conduct the study can strongly impact the conclusions. As such, a comprehensive review on this topic is highly desirable.

In this review, we will summarize recent investigations on the effects of external perturbation on the thermal properties of LD materials. This review focuses on the following external perturbation effects: mechanical strain, substrate interaction, and forming a cluster. Other effects such as bending and twisting are also briefly discussed. We try to establish a connection between different types of environmental perturbations and the variation in atomic structure, phonon dispersion, and anharmonic properties of LD materials. We believe that this review will further our knowledge about the perturbation effects on the thermal transport in LD materials and provide useful guidance for future investigations and practical applications.

General considerations

Crystal structure of low-dimensional materials

Because there are many LD materials, we will narrow our focus to a few representative ones, as summarized in Figure 1. CNTs and graphene are both allotropes of carbon [69]. Graphene has an one-atomic-thick honeycomb lattice structure with a C-C bond length of 1.42 Å [70]. Rolling a graphene sheet into a tube will yield a CNT [71]. The properties of a CNT depend on the rolling
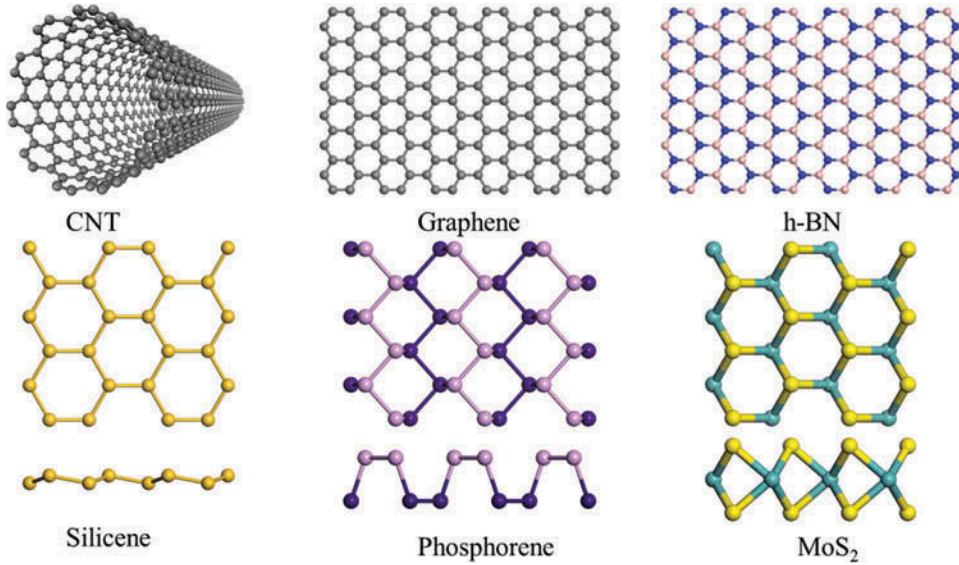
Figure 1. Atomic structures of different low-dimensional materials.

angle (chirality) and radius [71]. Hexagonal boron nitride (h-BN) has a lattice structure similar to that of graphene, except that it consists of alternating B and N atoms instead of carbon atoms [72]. The typical bond length for h-BN is 1.45 Å [73]. Silicene is the 2D silicon counterpart of graphene [74]. In comparison to graphene, freestanding silicene has a low buckled lattice structure; that is, the two atoms in a primitive cell are not arranged on the same plane [74]. The bond length is 2.2 Å and the buckling distance is ~0.45 Å [75]. Phosphorene is a 2D material consisting of phosphorus atoms [76]. It has a honeycomb-like puckered lattice structure, as shown in Figure 1. There are two types of bonds in phosphorene and the bond lengths are 2.22 and 2.26 Å [77]. MoS_2 is one typical transition metal dichalcogenide in which the Mo and S atoms are arranged in a sandwich structure by covalent bonds in a sequence of S-Mo-S [78]. The bond length of Mo-S bond is 2.42 Å [79]. Bi_2Te_3 QL is another 2D material that is composed of five atomic layers with a Te1-Bi-Te2-Bi-Te1 configuration and in each layer the atoms have a hexagonal arrangement [20]. Inside the quintuple layer, the Bi-Te2 bond is covalent and the Bi-Te1 bond is a combination of covalent and ionic interactions [20]. The thickness of the quintuple layer is ~1 nm [20]. In addition to inorganic materials, organic LD materials have attracted research interest in recent years. Polyethylene, the simplest and most widely used polymer, is synthesized by polymeric reaction of ethylene monomers (C_2H_4). According to the structural features, the abovementioned LD materials are classified into the following categories in this article: (1) 1D materials that contain CNTs, PE chains, etc.; (2) 2D pure-planar materials, including graphene and h-BN; (3) 2D nonplanar materials, including silicene, phosphorene, etc.; and (4) few-layer 2D materials, including MoS_2 (three layers) and Bi_2Te_3 QL (five layers).

Phonon transport theory

In nonmetal crystalline materials, the phonon gas model is generally used to describe the lattice thermal transport. A phonon can be treated as a quasiparticle that carries a certain amount of energy and transports in a certain direction with group velocity **v**. Under this framework, the transport of phonons can be described by the Boltzmann transport equation (BTE) [80]:

$$\frac{\partial f_\lambda}{\partial t} + \mathbf{v}_{g,\lambda} \cdot \nabla f_\lambda = (\frac{df_\lambda}{dt})_{scattering}, \tag{1}$$

where f_λ is the probability distribution function for a phonon mode labeled by λ, $\mathbf{v}_{g,\lambda}$ is the phonon group velocity, and the right-hand side of Eq. (1) is the scattering term that incorporates different scattering mechanisms. Under small perturbation, the nonequilibrium distribution function can be written as $f_\lambda = f_\lambda^0 + f_\lambda'$, where f_λ^0 is the equilibrium phonon distribution function and f_λ' is a temperature-independent small perturbation. If we further assume that the temperature gradient ∇T is small, the term ∇f_λ can be linearized and written as $\nabla T \cdot (\partial f_\lambda^0 / \partial T)$. At steady state Eq. (1) becomes

$$\mathbf{v}_{g,\lambda} \cdot \nabla T \frac{\partial f_\lambda}{\partial T} = \left(\frac{df_\lambda}{dt}\right)_{scattering}. \tag{2}$$

Single-mode relaxation time approximation is commonly used to solve this equation, in which a relaxation time τ_λ is assigned to each phonon mode, and the scattering term can be written as

$$\left(\frac{df_\lambda}{dt}\right)_{scattering} = -\left(\frac{f_\lambda - f_\lambda^0}{\tau_\lambda}\right). \tag{3}$$

Different phonon scattering mechanisms, including phonon–phonon scattering (p-p), phonon–impurity scattering, and phonon–boundary scattering, can be incorporated into the relaxation time through Matthiessen's rule:

$$\frac{1}{\tau_\lambda} = \frac{1}{\tau_{p-p}} + \frac{1}{\tau_{impurity}} + \frac{1}{\tau_{boundary}}. \tag{4}$$

When applying the expression for heat current and Fourier's law, the thermal conductivity can be expressed as

$$\kappa_{\alpha\beta} = \sum_\lambda c_\lambda \, v_{\lambda\alpha} \, v_{\lambda\beta} \, \tau_\lambda, \tag{5}$$

where c_λ is the lattice specific heat of mode λ, and $v_{\lambda\alpha}$ is the group velocity in direction α.

Phonon transport property of LD materials

Based on the phonon gas model and Eq. (5), the phonon dispersion curve plays an important role in determining the final thermal conductivity. For example, the mode-specific heat c_λ and the group velocity $\mathbf{v}_\lambda$ can be directly extracted from the dispersion curve. The dispersion curve is also important in determining the phonon lifetime because it determines the available phase space for phonon scattering [60, 81, 82]. For CNTs, due to the large number of atoms in a unit cell, the number of optical branches is extremely large, as shown in Figure 2a. Compared to the dispersion curve of bulk materials, one notable difference in 2D materials is the flexural acoustic branch instead of another transverse branch, as shown in Figure 2b, which represents the bending of 2D materials [83]. This flexural branch is mainly contributed by the out-of-plane atomic vibration. From the prediction of elasticity theory on layered materials, the shape of this flexural branch is quadratic at the long-wavelength limit [84–86]. The quadratic shape of the flexural branch was observed in purely planar 2D materials such as graphene [81] and h-BN [87]. For non-pure-planar or non-monolayer materials, such as silicene and MoS$_2$, both linear [75, 88] and quadratic [89, 90] behaviors of the out-of-plane (ZA) mode branch were reported. However, more recent studies show quite conclusively that the ZA branch of unstrained arbitrary 2D systems should also be quadratic [91–93]. The linear ZA branch reported in those materials is probably due to the inaccuracy in force constants and residual strain [92].

The phonon relaxation time in Eq. (5) is more complicated. For purely planar 2D materials, there is a selection rule for phonon scattering, which comes from the reflectional symmetry of the lattice [81]. Due to this selection rule, it is shown that any three-phonon scattering process must involve an
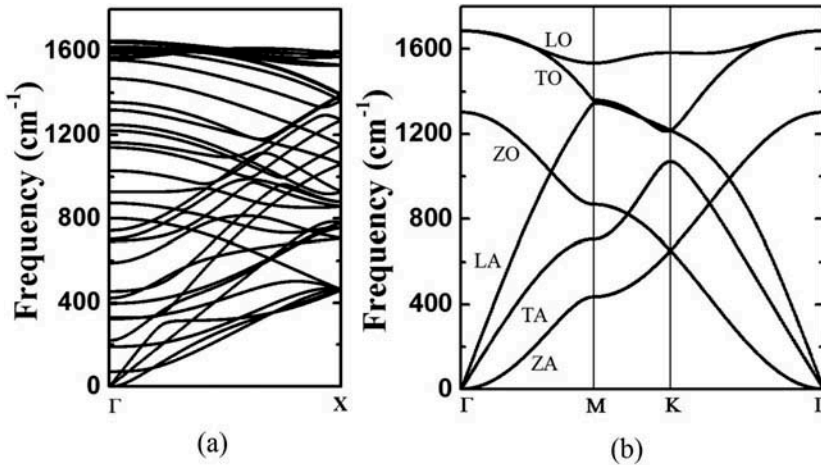
Figure 2. Phonon dispersion curve in (a) (5,5) CNT and (b) graphene.

even number of ZA phonons, which makes the scattering rate of ZA modes much smaller [81]. As such, ZA modes contribute a large part to the thermal conductivity in suspending graphene and h-BN [81, 87]. For 2D materials with few atomic layers, such as MoS_2, this selection rule is not strictly applicable, but the reflectional symmetry can partially reduce the scattering rate of those processes involve ZA modes [94, 95]. Some perturbations such as supporting on a substrate [61] or the interaction between other layers [96, 97] may also break the reflectional symmetry. Phonon–boundary scattering is another point worth mentioning. For three-dimensional bulk material, the phonon properties are assumed to be dominated by the vibrational behavior far away from boundary, so the phonon dispersion is not affected by the boundary. The boundary effect is thus regarded as an additional channel for phonon scattering and thus only reduces the phonon lifetimes. However, for LD materials, the boundary scattering term should be limited to the periodic dimension. If external perturbation is applied to the nonperiodic dimension, it not only affects the phonon lifetime but can also affect the structure and phonon dispersion curve [98, 99].

The aforementioned phonon–gas model and BTE-based theory only consider lattice thermal conductivity. We should note that thermal energy can also be carried by charge carriers [80]. For bulk material, lattice vibration is the major mechanism of thermal transport in semiconductor and insulators, whereas free electron contribution is dominating in metals [80]. It is, however, difficult to make such statements for LD materials. For example, CNTs can be metallic or semiconducting, depending on the chirality [100]. Perfect graphene is a semimetal, but it can open a bandgap when subject to some external perturbations [101, 102]. To date, a vast majority of recent research on environmental perturbations has focused on the impact on lattice conduction aspects, and the charge carrier thermal transport in many cases is often neglected. Therefore, we limit the scope of this article to the heat conduction by lattice vibration, but we also note that one should not simply assume that the charge carrier contribution to thermal conductivity is generally negligible in LD materials.

Computational and experimental methods

The investigations of thermal transport in LD materials are based on computational and experimental approaches. Among the computational methods, molecular dynamics (MD)-based approaches are still being widely used; for example, equilibrium molecular dynamics (EMD) [103] and nonequilibrium molecular dynamics (NEMD) [104]. The traditional EMD and NEMD methods can only obtain the overall thermal conductivity, and the mode-resolved thermal conductivity

information cannot be directly extracted. Recently, many computational approaches have been developed to extract mode-wise specific heat, group velocity, and relaxation time as in Eq. (5) from the interatomic interaction; most notably, the anharmonic lattice dynamics method based on perturbation theory [91, 105, 106] and normal mode analysis based on MD simulation [107–109]. The interatomic interaction can be extracted from either classical interatomic potential or the more accurate first principles calculations. Methods that can exactly solve Eq. (2) (the linearized BTE) without the relaxation time approximation have also been proposed [110, 111]. For most cases the exact solution of the linearized BTE gives results similar to the relaxation time approximation, but it is in principle more accurate, especially when the normal scattering process is important [30, 110, 111]. Each approach has its own advantages and disadvantages. All MD-based methods assume that the atomic system is purely classical, so the phonon distribution follows the Boltzmann statistics instead of Bose-Einstein statistics. In addition, MD simulations largely rely on the classical interatomic potentials because large simulation domains are required in these simulations. In the anharmonic lattice dynamics and direct solution of the linearized BTE, first principles calculations can be applied to obtain more accurate interatomic interactions (force constants). However, it can only deal with relatively simple periodic systems and usually neglects high-order anharmonicity to phonon scattering processes [112].

On the other hand, experimental characterizations of thermal properties are of the same importance to understanding thermal transport of aforementioned low-dimensional nanostructures. For instance, Raman thermometry is well introduced to the community by the first report of high thermal conductivity of monolayer graphene [8]. Because the temperature of materials is determined from the shift of its excited Raman peaks, the pros and cons are very distinct: for samples with an atomic layer structure such as graphene, its temperature response under laser excitation or electric heating can be probed directly. As such, the resolution for temperature measurement reaches the subnanometer scale in thickness direction [113], for which other characterization techniques are not comparable. The limitation comes from the resolution of the spectrometer, which determines the accuracy of temperature measurements. That is, when measuring samples with high thermal conductivity or interface materials with small thermal resistance, intensive heating supplied on the material is required to guarantee enough temperature rise and measurement accuracy [33]. A microbridge (microfabricated resistance thermometer) method is another well-developed technique with very wide thermal characterization applications from single CNTs [33, 114], CNT–CNT contacts [108], to graphene [61]. The measurement principle is very simple and employs Pt electrodes as thermometers and monitors the temperature variation during electrical heating based on a one-dimensional heat conduction model [108]. The challenge comes from the fabrication of samples to be measured, which requires high experimental skills and instrumentation to minimize the thermal/electrical resistance at the contact. When applied to the study of external perturbation on thermal transport of low-dimensional materials such as strain effect on thermal conductivity of graphene/CNTs, how to keep the sample stable during the measurement stage is the key aspect.

Strain effect

Strain is a description of deformation caused by external load or force. Depending on the direction of external force, it could include either tensile or compressive strain. For 2D materials, the strain can be uniaxial or isotropic, whereas for 1D materials the strain is usually applied in the axial direction. In fact, during the fabrication process, it is difficult to ensure a strain-free environment and LD materials will commonly have residual strain. On the other hand, there exists a set of techniques to tune the strain in LD materials [48], such as bending the flexible substrate, elongating the substrate, and local thermal expansion of the substrate [115, 116]. It is well known that strain has large effects on the electronic and optical properties of LD materials [48–50, 117]. For example, strain can open an electronic bandgap in graphene [102] or a direct–indirect–direct bandgap transition in phosphorene [118].

Under tensile strain, materials will be elongated. As a consequence, the interatomic distance, interaction force, and even crystal symmetry could be changed. For a pure planar 2D lattice, the symmetry will remain unchanged under isotropic strain but will be changed under uniaxial strain. For nonplanar 2D materials like silicene (buckled) and phosphorene (puckered), the lattice structure may also be changed and become more planar under tensile strain [60]. Any of the above factors will lead to a modification in the dispersion curve and hence thermal properties. For instance, the flexural branch in the dispersion curve of graphene becomes linearized under tensile strain [38]. In addition to the dispersion curve, the tensile strain could also alter the anharmonicity of the lattice, which will directly affect the phonon–phonon scattering [119]. On the other hand, due to the mechanical instability, LD materials can deform under compressive force. For example, CNTs and polymer chains will be bent under compressive strain [120] and graphene will become wrinkled [57, 121]. These structural deformations provide an additional channel for phonon scattering. Another consequence of the mechanical instability of an LD material under compressive strain is that the dispersion curve usually has negative frequencies [122]. In the following subsections, we will give a summary of recent findings of the strain effect on the thermal properties of LD materials.

Strain effect on graphene

Graphene is one of the most important LD materials since its discovery and has attracted most of the research efforts recently [8–10, 123, 124]. We will therefore first provide a review on the strain effects on graphene and then discuss other LD materials.

Compressive strain

Due to the mechanical instability, graphene will deform under compressive strain. It is experimentally found that wrinkles can form in graphene due to the thermally induced compressive strain [125, 126]. The wrinkled structure is also found in exfoliated monolayer graphene [127]. A similar phenomenon is also observed in some MD simulations [57, 121]. More recently, it has been experimentally demonstrated that the crumpling and unfolding of large-area graphene could be controlled through a prestretched polymer substrate [128]. The question is how the strain-induced wrinkles will affect the thermal properties of graphene.

MD simulations have been widely used to investigate this problem. For example, Li et al. found that isotropic compressive strain (in-plane, biaxial) induces buckling in graphene sheets [57]. EMD results show that an 8% compressive strain leads to a 46% reduction in the thermal conductivity [57]. This reduction is attributed to the more irregular surface induced by larger strain and stronger phonon scattering. Wei et al. used an NEMD method to calculate the strain effect (uniaxial) on the thermal conductivity [121]. They found a smaller reduction (less than 10%) in thermal conductivity when a 10% compressive strain is applied [121]. The fact that the existence of wrinkles or buckling will introduce phonon scattering and lead to a reduction in the thermal conductivity is also supported by experimental measurements. Chen et al. [129] measured the thermal conductivity of suspended graphene membranes by micro-Raman mapping and found that the average thermal conductivity of graphene membranes without wrinkles is 1,875 ± 220 W/mK, which is ~27% higher than that of membranes with wrinkles. The existence of a temperature rise at the wrinkle structure has also been experimentally observed by scanning Joule expansion microscopy, as shown in Figure 3, which indicates more frequent phonon scatterings at the wrinkle structure [130].

Tensile strain

Tensile strain will affect the thermal transport in graphene from different aspects; that is, through modification of the phonon dispersion curve [39] and the lattice anharmonicity [131]. The former factor can affect the phonon group velocity, specific heat capacity, and phonon relaxation times, and the latter factor affects phonon relaxation times. Research has shown that tensile strain can soften the in-plane longitudinal acoustic (LA) and transverse acoustic (TA) modes, whereas the ZA mode
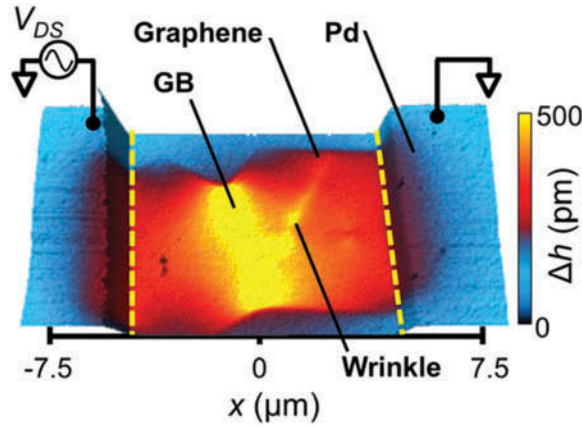
Figure 3. Scanning Joule expansion microscopy image of a wrinkled graphene. Δh refers to the surface expansion, which is proportional to the temperature rise ΔT. Larger Δh occurs at the grain boundaries and wrinkles in the graphene, which means that there are large temperature increases at these regions. Adapted from Grosse et al. [130] with permission.

become stiffened and linearized [38, 53, 57, 59]. Nevertheless, the effect of tensile strain on the thermal conductivity of graphene is still far from conclusive [39, 132, 133].

In some studies, it was reported that the thermal conductivity of graphene is reduced under tensile strain. For example, through molecular dynamics and Green-Kubo methods, Li et al. found that the thermal conductivity of graphene would be reduced under tensile strain (uniaxial). An 8% tensile strain leads to a 42% reduction in thermal conductivity [57]. The reduction in thermal conductivity under tensile strain is explained by the variation in the phonon dispersion curve under tensile strain [57]. Wei et al. also applied NEMD simulations to investigate the strain effect on the thermal conductivity of graphene ribbons and similar reductions in thermal conductivity were reported [121]. For example, thermal conductivity in 10-nm-long zigzag graphene nanoribbons could be reduced by 60% when the applied tensile strain reaches 20% [121]. The reduction in thermal conductivity is also explained by the softening of phonon mode under tensile strain. Ma et al. [122] also found a reduction in thermal conduction in graphene caused by tensile strain, in which the thermal conductivity is calculated from the BTE within the single-mode relaxation time approximation (RTA) and the average Gruneisen parameter is taken to calculate the phonon–phonon scattering rate.

In some other studies it was reported that the thermal conductivity diverges under tensile strain. The main argument for the divergence of thermal conductivity is the abnormal behavior of long-wavelength ZA modes under tensile strain. Through first principles–based methods, Bonini et al. [38] showed that the TA and LA phonons in freestanding graphene display finite lifetimes in the long-wavelength limit (hence the mean free path will be smaller than the wavelength in this limit), making them ill-defined as elementary excitations. Mechanical strain will linearize the ZA dispersion curve. As shown in Figure 4, the unstrained dispersion of flexural mode is purely quadratic, and the dispersion under strain clearly has a finite slope (linearized) near the zone center. Bonini et al. showed that the linearization of ZA branch has two major consequences [38]. First, the decay rate of in-plane acoustic modes (TA/LA) changes from a constant to a q^3 (here q is the norm of the wave vector) dependence near the zone center and thus makes all phonons well defined. Second, the ZA + ZA → TA/LA absorption process for ZA modes changes from q^2 dependence to q^3 dependence, which makes the contribution of ZA modes diverge logarithmically with length. The divergence of thermal conductivity in strained graphene is also partly supported by Pereira and Donadio [39]. Through EMD simulation and Green-Kubo methods, they showed that the thermal conductivity of unstrained graphene is finite and converges with size at finite temperature [39]. In contrast, when the applied strain is larger than a threshold value of 2%, the thermal conductivity of the strained graphene diverges logarithmically with time, as shown in Figure 5. Again, the divergence of
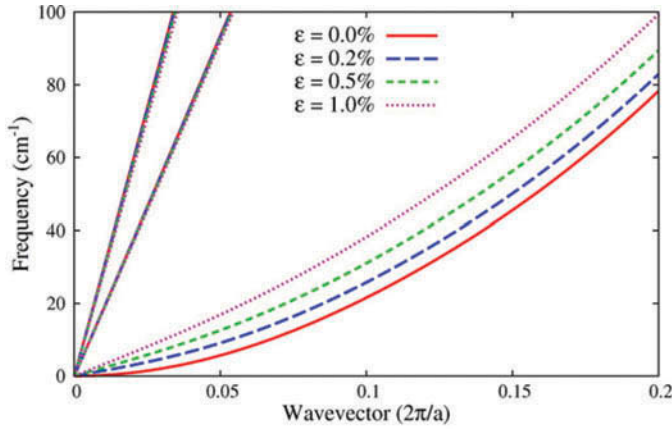
Figure 4. Phonon dispersion curves of acoustic modes in graphene around the zone center under different tensile strains ε. The lowest branch is the ZA branch and it changes from quadratic to linear under tensile strain. Adapted from Bonini et al. [38] with permission.
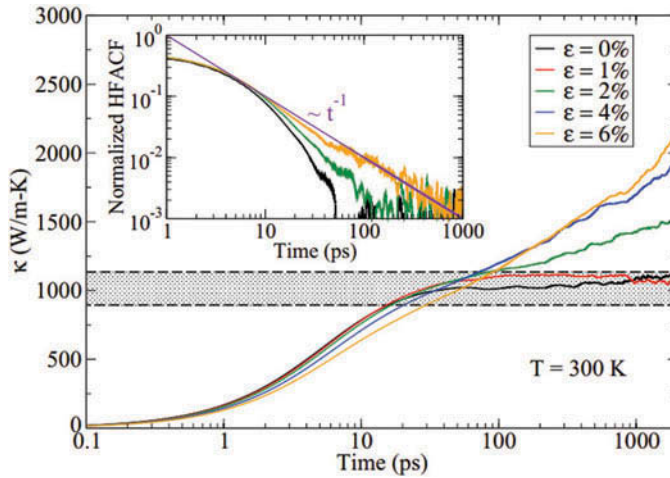

Figure 5. Integrated thermal conductivity of strained graphene calculated from the Green-Kubo method at 300 K. When the strain is relatively small (less than 2%), the thermal conductivity is converged. However, the thermal conductivity diverges as the strain increases (larger than 2%). Inset: the heat current autocorrelation function corresponding to different tensile strain. Adapted from Pereira and Donadio [39] with permission.

thermal conductivity is due to the increase in lifetime of long-wavelength ZA modes. Through a time domain modal analysis, Gill-Comeau and Lewis also reported a divergence in thermal conductivity at moderate (4%) strain [124]. The divergence in thermal conductivity is also attributed to the linearization of long-wavelength ZA modes under tensile strain [124]. Based on the exact solution of BTE with the force constants calculated from first principles, Fugallo et al. showed that isotropic tensile strain has a relatively weak effect (the variation is within 10%) on thermal conductivity of graphene, which is also valid for the case of infinite graphene [132]. In addition, they also showed that the results from the relaxation time approximation provide a large increase in thermal conductivity with tensile strain, and the thermal conductivity is diverged for infinite size graphene [132].

In reality we are always concerned with crystals of finite dimensions. For a finite size system, the long-wavelength ZA modes that may cause the divergence of thermal conductivity can be effectively

scattered by the boundary, and the thermal conductivity is always finite. When considering the boundary scattering, Lindsay et al. [131] solved the BTE iteratively with the interatomic force constants obtained from first principles calculations and found that a 1% isotropic tensile strain has a negligible effect on the thermal conductivity when the system size ranges from 1 to 50 μm. This result is also consistent with the results of Fugallo et al. [132].

There is also research on the strain effect of multilayer graphene. Kuang et al. [58] studied the thermal conductivity of few-layer graphene (bilayer and trilayer) under different isotropic tensile strains by a first principles–based BTE method. It was found that with an increase in strain, the thermal conductivity of few-layer graphene will first increase and then decrease. A 4% tensile strain could lead to an ~40% increase in the thermal conductivity of bilayer graphene. A deeper analysis shows that this nonmonotonic dependence of thermal conductivity on strain is the result of two competing effects: the relaxation times of ZA modes increase with strain and the heat capacity of low-lying ZA modes decreases with strain. With an increase in strain, the magnitude of anharmonic interatomic force constant is reduced, which results in an increase in ZA mode relation times. The linearization of zone center dispersion of the ZA branch is responsible for the reduction in mode heat capacity. Later, Zhang et al. [134] applied NEMD simulations and found that the thermal conductivity of a functionalized bilayer graphene sheet can be enhanced by tensile strain.

Based on the existing literature, the thermal conductivity of graphene is reduced under compressive strain, which is originated from the mechanically unstable nature of LD materials under compression. Structural deformations such as wrinkles appear in graphene under compressive strain and will induce additional phonon scattering. Such a trend is observed in both theoretical calculations and experimental characterizations. On the other hand, the tensile strain effect on graphene remains inconclusive. Most investigations of tensile strain effects on graphene are theoretical. Depending on the geometry, investigation methods, and types of applied strains, the tensile strain effect may be different. From our perspective, the discrepancies between different research works are likely to arise from the different treatment of the zone center long-wavelength phonons. It seems that a full solution of the linearized BTE shows that the thermal conductivity does not significantly depend on strain, whereas relaxation time approximation gives a diverging thermal conductivity. For MD-based approaches, EMD results with a large simulation domain seem to support a diverging thermal conductivity with strain, but NEMD shows a reduction in thermal conductivity. Each method has its own problems, so it is difficult to achieve a conclusion at this stage. A summary of different investigations on tensile strain effects is given in Table 1.

Strain effect on other low-dimensional materials

Other low-dimensional materials, such as CNTs, polymer chains, silicene, MoS_2, and black phosphorene, have also attracted much interest recently. There are some recent studies about the strain effects on these materials, which will be reviewed in this section.

Table 1. Effect of tensile strain on the thermal conductivity of graphene.

| Geometry	Method	Strain	Effect	Reference
Infinite (periodic)	Green-Kubo	Uniaxial	Reduce	[57]
10-nm-long nanoribbon	NEMD	Uniaxial and biaxial	Reduce	[121]
3 μm wide	BTE (RTA)	Uniaxial	Reduce	[122]
Infinite	BTE (RTA)	Isotropic	Diverge	[38]
Infinite (periodic)	EMD	Uniaxial	Diverge	[39]
Infinite (periodic)	EMD (modal analysis)	Isotropic	Diverge	[124]
1–50 μm wide	BTE (exact solution)	Isotropic	Insensitive	[131]
Two to four layer infinite	BTE (exact solution)	Isotropic	Enhance	[58]
Finite and infinite (periodic)	EMD and NEMD	Uniaxial	Reduce	[59]
Both finite and infinite	BTE (exact solution)	Isotropic	Insensitive	[132]
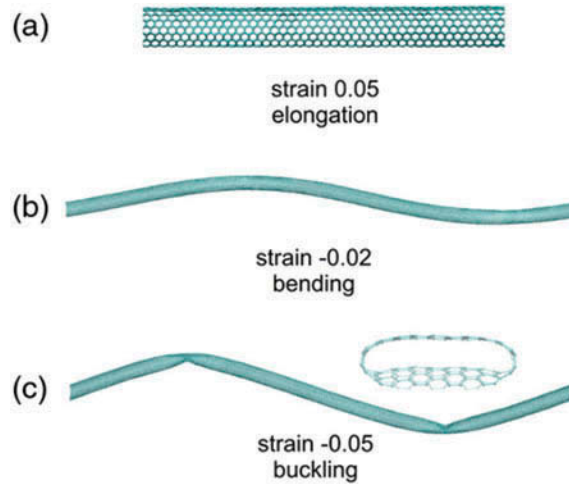
Figure 6. Response of CNT under tensile and compressive strain. (a) CNT will be elongated along the axial direction but remains the tubular geometry under tensile strain. (b) When compressive strain equals −2%, buckling occurs in the CNT. (c) At higher compressive strain (−5%), the bulking in CNT collapses into a flat cross section. Adapted from Xu and Buehler [120] with permission.

Carbon nanotube

Using NEMD simulations methods, Xu and Buehler [120] systematically investigated the strain effect on the thermal conductivity of single-walled CNTs. Compared to the thermal conductivity value without strain, they found that either tensile strain or compressive strain will lower the thermal conductivity of CNTs [120]. Under tensile strain, the carbon–carbon bonds will be elongated, as shown in Figure 6a. As a consequence, the phonon mode is softened and thus the phonon group velocity decreases; therefore, the thermal conductivity is decreased. When the tensile strain approaches the failure limit, the thermal conductivity reduces to approximately 70%. This situation is basically similar to what has been observed in bulk materials [56]. Due to the structural instabilities of CNTs, the thermal conductivity will still be reduced under compressive strain. As shown in Figures 6b and 6c, the CNT buckles under compression; the localized buckling will lead to strong phonon scattering and hence the thermal conductivity is reduced [120]. A 5% compressive strain leads to a 32% reduction in thermal conductivity. Li et al. [57] also conducted NEMD simulations to investigate the strain effects on the thermal conductivity of CNTs. The deformation of CNTs under compressive strain is also observed and hence the thermal conductivity reduces after the strain reaches a certain amount.

Polyethylene chains

Due to the mechanical instability and low stiffness of 1D polyethylene chains, their morphology will be changed under both compressive and tensile strain. Applying compressive strain could result in wavy geometry of the chain, which dramatically increases the wiggles and segmental rotations and thus leads to much more phonon scattering and a huge reduction in thermal conductivity. In contrast, tensile strain increases the stiffness and improves the lattice order, thus enhancing the thermal conductivity. Using NEMD simulations, Zhang and Luo [135] found that the thermal conductivity of a single polyethylene chain increases by ~50 times (from 3.69 to 181.28 W/mK) as the strain increases from −0.2 to 0.2. The authors concluded that stretching results in better lattice order and less phonon scattering. Experimental measurements by Shen et al. [16] confirmed that the thermal conductivity of PE nanofibers increases with increasing draw ratios and reaches values as high as ~104 W/mK.

Silicene

Silicene is the two-dimensional silicon-based counterpart of graphene with a honeycomb lattice structure. Different from the pure planar structure of graphene, a slight buckling exists in free-standing silicene [74]. Hu et al. [53] investigated the thermal transport in silicene sheets under uniaxial stretching (zigzag direction) through NEMD simulations. They found that the thermal conductivity of silicene and silicene nanoribbons first increases significantly with applied tensile strain and then fluctuates at an elevated plateau. Pei et al. also investigated the strain effect on the thermal conductivity of silicene through NMED simulations [136]. They found that the thermal conductivity of silicene increases at small tensile strain but decreases at large strain. This tensile response is different from the result observed by Hu et al. [53]. Different empirical potentials may be the reason for the different tensile strain response of silicene.

Instead of using classical potentials and MD simulations, more convincing results can be obtained based on first principles calculations and iterative solution of the linearized Boltzmann-Peierls equation. Similar to graphene, there is also argument about the possible divergence of thermal conductivity of silicene [60, 75, 137, 138], and the results are still not conclusive. To avoid this argument, Xie et al. calculated the thermal conductivity of finite size silicene under isotropic tensile strain, which exclude the long-wavelength phonons that could lead to possible divergence [60]. They found that the thermal conductivity of silicene increases dramatically with strain and then decreases. Depending on the size, the maximum thermal conductivity of strained silicene occurs at about 4% strain and the value can be a few times larger than that of the unstrained case [60], as shown in Figure 7a. The dramatic increase in thermal conductivity is mainly due to the increase in acoustic phonon lifetime, and the variation of specific heat and group velocity have a quite small effect on the results (note the difference from the case of graphene). Careful analysis shows that the flattening of the silicene structure under tensile strain plays an important role in the increase of acoustic phonon lifetime [60]. As shown in Figure 7b, with an increase in tensile strain, the bond length between atoms is increased and the buckling distance is decreased. The fact that the structure is becoming more planar can significantly reduce the coupling of flexural acoustic modes with the in-plane phonon modes, which makes the scattering rates among these modes significantly reduced [60]. Using a similar method, Kuang et al. [138] also found that the thermal conductivity of silicene could increase with strain.

MoS$_2$

There are also some studies about the strain effect on the thermal transport in MoS$_2$. By a combination of first principles calculations and BTE, Zhu et al. [119] investigated the biaxial tensile
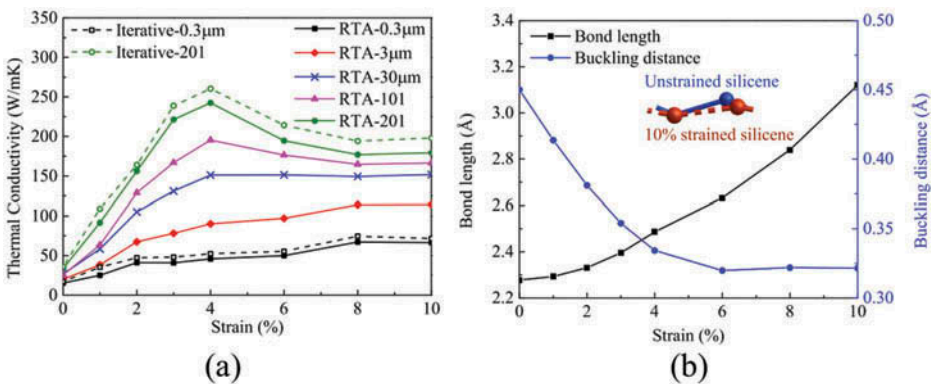

Figure 7. (a) Thermal conductivity of silicene under tensile strain with different sizes or different meshes for Brillouin zone integration (b). Bond length and buckling distance in silicene under different strain. Adapted from Xie et al. [60] with permission.

strain effect on the thermal transport properties in MoS$_2$. They found that the thermal conductivities of single-layer MoS$_2$ could be suppressed by the applied strain. A biaxial tensile strain (2–4%) could result in a 10–20% reduction in thermal conductivity. Again, this is explained by the acoustic mode softening under strain, which leads to much smaller group velocity in strained MoS$_2$. They also found that the amount of reduction in thermal conductivity is size dependent. For example, for a 10 nm size sample, the amount of reduction in thermal conductivity is 15% when the tensile strain is 5%. In comparison, the same amount of strain leads to a 25% reduction in thermal conductivity when the sample size is 1,000 nm. The amount of reduction saturates when the sample size is larger than 1,000 μm. Through NEMD simulations, Ding et al. also found that tensile strain can lead to a reduction in thermal conductivity in MoS$_2$ [139]. Similarly, the reduction in thermal conductivity is mainly attributed to the strain-induced phonon mode softening [139]. Here we comment that although phonon softening is generally used to interpret the simulation results, these research works need to also carefully examine the effect of strain on phonon relaxation time. The softening only refers to the group velocity, which may not be fully responsible for the reduction in thermal conductivity. The phonon relaxation time could also play an important role.

Substrate effect

The structure of LD materials supported on a substrate, as shown in Figure 8, is a typical configuration in many applications [3, 17, 142, 143]. Many LD materials are directly grown on substrates so they are naturally in the supported form. For instance, graphene may grow on copper [144] and silicon carbide substrate [145], and silicene could be grown on Ag substrate [146]. On the other hand, the LD materials need to be supported on a substrate in most applications. For example, when an LD material acts as a conductive channel in a field effect transistor [2, 3, 18]. In some optoelectronic devices, graphene is supported on a substrate to act as a transparent layer [147, 148]. The substrate can be different in material types and crystallinity (e.g., crystalline,
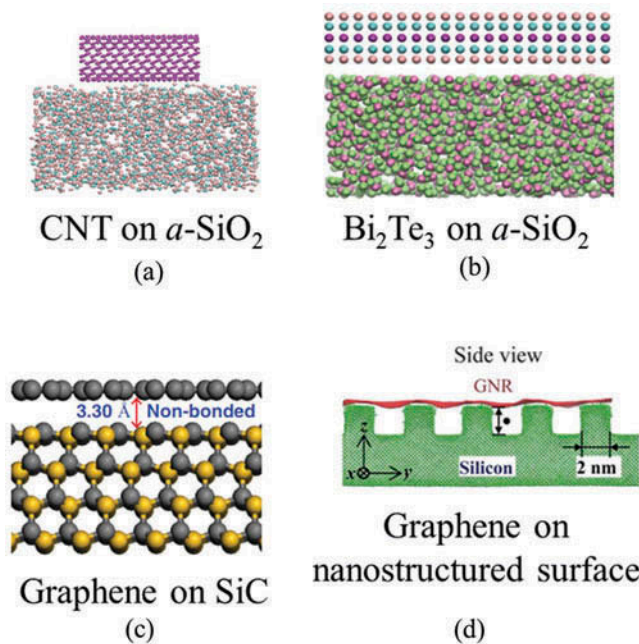

Figure 8. Low-dimensional materials supported on different types of substrate. Parts (c) and (d) are adapted from Guo et al. [140] and Zhang et al. [141] with permission.

polycrystalline, or amorphous). The morphology at the surface of the substrate could also be quite different. It could be atomically smooth, rough, or periodically nanostructured. Moreover, the interaction between the substrate and supported LD materials can be van der Waals interaction, covalent bonding [149], or a mixture of both types. It is also experimentally demonstrated that the interaction between the substrate and the supported LD materials could be tuned in a wide range by intercalation of atoms [150–152].

Once the LD materials are placed on a substrate, the interaction force with the substrate can influence the thermal properties of the LD materials. There are different views on the effects of the substrate on the supported materials. In some studies, the substrates are treated as an external on-site perturbation to the LD materials [153, 154]. The dispersion curve of the supported materials is assumed to be unchanged and the substrate only induces additional phonon scattering. In some other studies, the substrate and the supported materials are treated as a whole and their dynamics are assumed to be coupled [155]. For instance, the surface Rayleigh wave, which is one type of surface elastic wave, may have some influence on the dynamics of the supported materials [156]. Some studies show that the flexural modes in supported 2D materials may couple with the surface Rayleigh wave and form coupled vibrational modes [155]. This type of coupling may lead to the linearization and up-shift of the flexural phonon branch for supported material and hence affect its thermal transport properties [155, 156]. When the surface of the substrate is nanostructured (pillar, periodic trench), the nonuniform interaction force from the substrate may cause the deformation of the supported materials [157–159]. Similar to strain-induced deformation, it induces additional phonon scattering and hence affects the thermal properties. In the following subsections we provide a detailed review on the substrate effects.

Substrate effect on graphene

The first experimental measurement on thermal transport property of supported graphene was carried out by Seol et al. [61]. Using the microbridge method, they found that the thermal conductivity of supported graphene on an a-SiO$_2$ substrate is about 600 W/mK at room temperature, which is significantly lower than the reported value for freestanding graphene (~3,000–5,000 W/mK from Raman measurement [8]). To gain better insight, the authors adopted a theoretical model to explain the substrate effect on thermal conductivity. In this theoretical model, the phonon–phonon scattering rate was obtained by first principles calculations for a freestanding graphene and the substrate effect was considered as a boundary scattering term, in which the scattering rate of each mode was assumed to be proportional to the square of coupling strength and inversely proportional to square of phonon frequency [61]. The experimental data can be reproduced from the theoretical model when assuming that the substrate scattering rate of ZA mode is much stronger than that of the LA and TA modes, indicating that the strong scattering of the ZA mode is probably the reason for the large reduction in thermal conductivity of supported graphene. The thermal conductivity of supported graphene was also measured by Cai et al. using a different approach [36]. The graphene sample was grown by chemical vapor deposition on copper and then transferred to an Au-coated substrate [36]. Through Raman measurement, they found that the thermal conductivity is (370 + 650/−320) W/mK [36], which is in agreement with the measurement of exfoliated graphene supported on a-SiO$_2$ [61]. Inspired by these experimental results, simulation works were conducted to interpret the physical mechanism underlying thermal transport in supported graphene. Through MD simulations with the phonon normal mode analysis, Qiu and Ruan [63] compared the phonon properties of a freestanding graphene and a graphene supported on an a-SiO$_2$ substrate. They found that the phonon dispersion curves for the two cases are nearly identical, as shown in Figure 9a. The phonon relaxation times of all phonon branches are reduced when it is supported on the substrate, as shown in Figure 9b, among which the relaxation times of ZA modes have the most obvious reduction. The reason for the reduction inphonon relaxation time is attributed to the interfacial
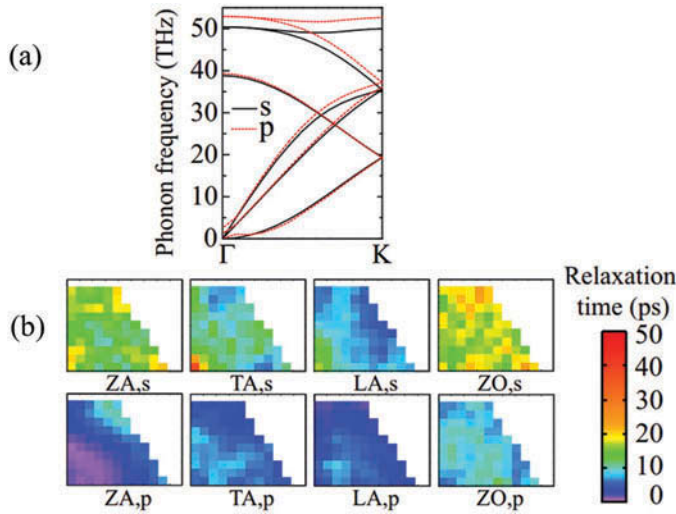
Figure 9. (a) Phonon dispersion curve and (b) phonon relaxation times in the irreducible Brillouin zone for freestanding and supported graphene from MD simulations. The subscripts s and p are short for suspended and supported, respectively. Adapted from Qiu and Ruan [63] with permission.

scattering and the breaking of reflectional symmetry. However, the overall reduction in thermal conductivity is not provided in this work.

Similar to Qiu and Ruan [63], Ong and Pop [155] also examined the thermal transport of a-SiO$_2$ supported graphene through MD simulations. They showed that coupling to the substrate leads to an order of magnitude reduction of thermal conductivity and attributed this effect to the damping of the flexural acoustic phonons. They further examined the effect of coupling strength and found that the thermal conductivity does not monotonically depend on the coupling strength. The thermal conductivity of graphene first decreases with coupling strength and then increases. Detailed analysis shows that the surface Rayleigh wave of the substrate could couple with graphene and thus modify its vibrational property [156]. As shown in Figure 10, the substrate Rayleigh wave is a type of surface elastic wave that exists at the surface of a substrate. When a thin layer is adsorbed on the substrate, the out-of-plane vibration of the thin layer can couple with the surface Rayleigh wave and thus affect its vibrational property. Based on this understanding, Ong and Pop [155] examined the dispersion relation in a continuum model of an ideal graphene membrane supported on an isotropic elastic substrate. With an increase in coupling strength, they observed the formation of two hybridized linearized modes with higher group velocities, as shown in Figure 11. Through a simple continuum model, it is found that the increased thermal conductivity of supported graphene with an increase in
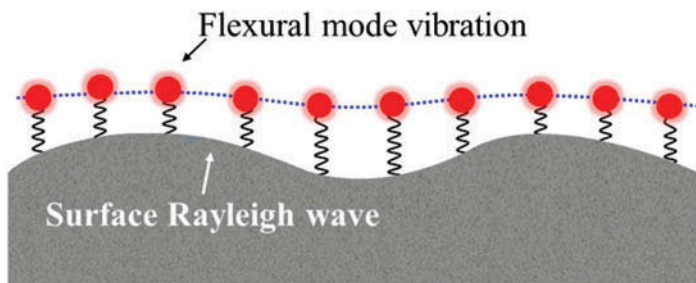

Figure 10. Illustration of the coupling between flexural mode of a 2D material and surface Rayleigh wave of the substrate.
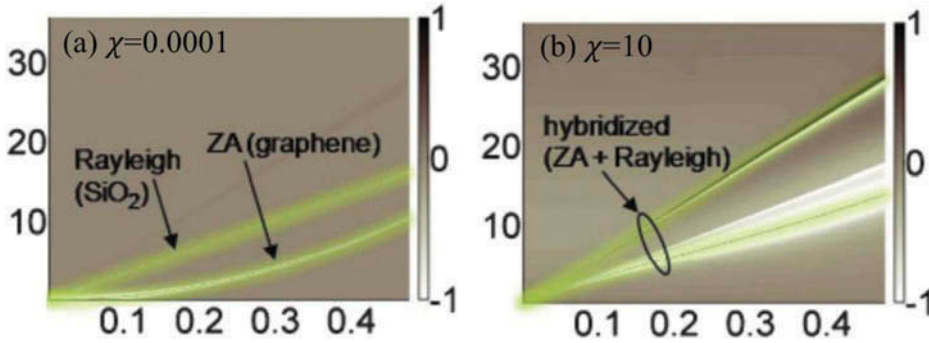
Figure 11. Zone center phonon dispersion curve calculated from MD and normal mode analysis method, in which χ denotes the coupling strength. (a) When the coupling strength is weak, the dispersion curve for the Rayleigh wave is linear, and the ZA branch is quadratic. (b) With strong coupling strength, the dispersion curves of the two modes are hybridized. Adapted from Ong and Pop [155] with permission.

coupling strength is a consequence of the linearized higher velocity elastic waves at the graphene/a-SiO$_2$ interface.

Graphene could also be epitaxial grown on SiC substrate [160], and unlike the case of exfoliated or transferred graphene supported on an a-SiO$_2$ substrate, the interaction between epitaxial growth graphene and SiC substrate could be more complicated. In experiments, both covalent bonding and weak van der Waals interactions are observed at the interface [145, 161]. Motivated by these factors, Guo et al. investigated the thermal transport in graphene supported on an SiC substrate with different interactions on the surface using an NEMD method [140]. For the case of a weak van der Waals interface, the thermal conductivity is reduced by 20% compared to the suspended one, and strong covalent bonding could lead to a more than 90% reduction in thermal conductivity [140]. Thermal properties of graphene supported on SiC substrate are also investigated through a method that incorporates first principle calculations and the nonequilibrium Green's function method [162]. In this work, the authors studied the configuration in which two graphene layers are supported on an SiC substrate, and a 35% reduction in thermal conductance was observed in the graphene layer closest to the substrate [162]. The effect of silicon substrate on graphene was also investigated by Wei et al. [163]. Through the normal mode analysis, they found an ~40% reduction in thermal conductivity of supported graphene, which is similar to previous studies [163]. They also showed that the reduction in thermal conductivity can reach 70% by enhancing the coupling strength by five times [163].

Chen et al. studied another aspect of substrate effect on the thermal transport of graphene using NEMD simulation [164]. For suspended graphene, they studied the thermal conductivity using different length of simulation domain and found strong length dependence in thermal conductivity, which is normal for NEMD simulations. However, in supported graphene they found that this length dependence is largely suppressed [164]. It is found that the long mean free path flexural mode in suspended graphene is the reason for its strong size dependence. Coupling to the substrate causes damping of the flexural modes, which suppresses the size effect in supported graphene.

In addition to monolayer graphene, the thermal conductivity of supported multilayer graphene has also been investigated. Sadeghi et al. [54] measured the in-plane thermal conductivity of graphene samples on a-SiO$_2$. They found that the thermal conductivity of supported multilayer graphene increases with the number of layers in the range between 1 and 34 atomic layers, and even for the thickest one (34 atomic layers) the thermal conductivity is still lower than that of a natural graphite sample [54]. The authors explain the results as follows: First, the mean free path of phonons in graphite is long along the basal plane and cross-plane directions. Second,

phonon scattering at the multilayer graphene–amorphous support interface is quite diffuse, which affects the overall thermal conductivity. Such a result is consistent with the MD simulation results from Chen et al., in which they found that the thermal conductivity of MLG saturates at a thickness of 40 layers [164]. Liu et al. measured the thermal conductivity of single- to few-layered graphene supported on an organic substrate (poly methylmethacrylate) by using a transient electrothermal technique [165]. The values range from 33.5 to 365 W/mK with layer numbers from six to one, which are significantly lower than that of supported graphene on a-SiO$_2$ [165]. They attributed this property partially to more phonon scattering induced by the substrate effect and partially to the intrinsic poor quality of graphene due to the oxidation effect. Recently, a two-step Raman thermometry has been developed by Zhao et al. to measure the interfacial thermal conductance between graphene and a-SiO$_2$ and the thermal conductivity of graphene [166]. The authors believe that if phonon scattering in graphene due to the substrate effect is enhanced, the interfacial thermal conductance would be improved as a matter of stronger interaction [166]. This new technique could provide a pathway for future comprehensive investigations regarding how thermal transport of graphene is influenced by substrate interaction quantitatively.

Substrate effect on other low-dimensional materials

Silicene

Silicene has a lattice structure similar to that of graphene except that it is buckled. By MD and spectral energy density analysis, Wang et al. [167] investigated the thermal conductivity and spectral phonon properties of freestanding and supported silicene through normal mode analysis. Similar to graphene, an a-SiO$_2$ substrate results in a 78% reduction in thermal conductivity at 300 K. Note that they employed the Tersoff potential for silicon to model silicene, which results in a problematic planar structure. Zhang et al. [64] investigated the substrate effect of silicene using a similar method but a refined Stillinger-Weber (SW) potential. In addition, unlike the amorphous substrate considered by Wang et al., the authors considered a crystalline SiC substrate. They found that the thermal conductivity of silicene is enhanced on a 6H-SiC substrate and suppressed on 3C-SiC [64]. They explained the anomalous phenomenon to the substrate effect on the phonon relaxation time. In the case of 6H-SiC substrate, the dramatic increase in thermal conductivity is due to the augmented lifetime of the majority of the acoustic phonons [64]. For the cases of 3C-SiC substrate, the reduction in lifetime is due to the reduction in the lifetime of almost the entire phonon spectrum [64]. However, based on the spectral energy density plot, as shown in Figure 12, it seems that the phonon dispersion curve of silicene is also strongly modified by the SiC substrate. In particular, the low-frequency flexural branch seems to be diminished for the supported silicene. The surprising results could also be related to the modification in phonon dispersion instead of just phonon relaxation time.

Bi$_2$Te$_3$ quintuple layer

Bi$_2$Te$_3$ is a quasi-2D material consisting of five atomic layers. Compared to graphene and silicene, it has more atomic layers, heavier atoms, and extremely low intrinsic thermal conductivity. Through MD simulations and normal mode analysis, Shao and Bao [109] found that supporting on a substrate leads to an ~50% reduction in the thermal conductivity. The coupling with an a-SiO$_2$ substrate has a twofold effect on the thermal properties of the supported QL. First, the existence of an amorphous substrate could cause additional scattering channels for all of the phonon modes in QL. As a consequence, the phonon relaxation times in the supported QL will be reduced compared to the freestanding one. Second, the low-lying flexural mode in supported QL is up-shifted and flattened, which is a consequence of coupling with the substrate Rayleigh modes. It should be noted that a similar flattening of flexural modes in supported materials is also observed in graphene [156].
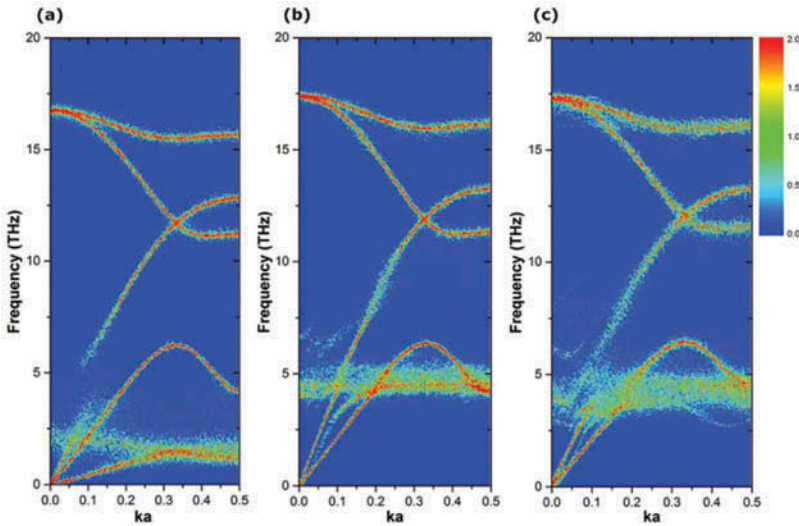
Figure 12. Phonon spectral energy densities of (a) freestanding silicene and silicene supported on (b) 6H-SiC substrate and (c) 3C-SiC substrate. Adapted from Zhang et al. [64] with permission.

Carbon nanotubes

Carbon nanotubes have a cylindrical geometry instead of a planar one. When supported on a substrate, only part of the atoms in CNTs interact with the substrate, which makes it quite different from the case of 2D materials. Therefore, the substrate effects for 2D materials cannot be directly applied to CNTs. Through MD simulations and normal mode analysis, Ong et al. [62] investigated the thermal properties of (10, 10) CNTs supported on a-SiO$_2$ substrate. The thermal conductivity of supported CNTs is found to be ~33% lower than that of suspended CNT. By comparing the relation between scattering rates and the displacement in the eigenvector, the authors suspect that the substrate is more likely to scatter phonon modes with radial atomic displacements. Using NEMD simulations, Qiu et al. [168] also investigated the thermal transport in suspended and supported CNTs. A 34–41% reduction in thermal conductivity was observed when supported on an a-SiO$_2$ substrate, which is similar to the prediction of Ong et al. [62]. It should also be mentioned that the supported CNTs can undergo large deformations due to the van der Waals interaction with the substrate [169], which has not been carefully discussed in those simulation works. In contrast to the case of graphene, experimental studies of the substrate effect on CNT are still missing.

In Table 2 we provide a summary of substrate effects on the thermal conductivity of different supported materials. All of these investigations are based on the same approach; that is, MD and normal mode analysis.

Effect of nanostructured surfaces

Instead of supporting on a smooth surface, some studies have been carried out to investigate the effects of nanostructured surfaces on the thermal properties of supported materials. For example, Mi et al. fabricated an array of SiO$_2$ nanopillars through a self-assembled block copolymer [158]. It was found that a biaxial tensile strain was generated when the graphene sheet was transferred to the surface [158]. Through MD simulations, Zhang et al. found that the subnanometer roughness on the Si surface could increase the coupling strength between the graphene layer and the substrate, which is contrary to the traditional expectation [141]. A deeper analysis shows that the interfacial C-Si bond could be tuned by the surface roughness, which is the main reason for the enhancement in the coupling strength between the graphene and Si substrate [141]. Sevincli and Brandbyge investigated

Table 2. Summary of substrate effects on the thermal conductivity of supported materials.

Material	Substrate	Effect	Remark	Reference
Graphene	a-SiO$_2$	Reduced	—	[61]
Graphene	a-SiO$_2$	Reduced	—	[63]
Graphene	a-SiO$_2$	Reduced	Thermal conductivity could be tuned by the coupling strength	[155]
Graphene	SiC	Reduced	—	[162]
Graphene	Si	Reduced	—	[163]
Silicene	a-SiO$_2$	Reduced	—	[167]
Silicene	SiC	Bilateral	Depending on the surface crystal plane	[64]
Bi$_2$Te$_3$ QL	a-SiO$_2$	Reduced	—	[109]
CNT	a-SiO$_2$	Reduced	—	[62, 168]

the effects of an abrupt kink in the substrate on the thermal conductance of supported graphene through the Green's function method [157]. It is found that the abrupt kink in the substrate will induce bending in the supported graphene, which is detrimental for the thermal transport in graphene [157]. These research works show that the nanostructured surface can induce strain, tune the coupling strength, and change the atomic structure of LD materials. It can be expected that the nanostructured surface can affect the thermal properties of the supported LD material, and the mechanism could be more complicated than a planar substrate. However, research on such effects is relatively few.

Clustering

As shown in Figure 13, many LD materials tend to form a cluster, such as multiwalled CNTs [33], CNT bundles [170], polymer nanofibers [171], and few-layer graphene [172]. For example, for CNT-based thermal interface materials, multiwalled carbon nanotube (MWCNT) and CNT bundles instead of single freestanding CNTs are more commonly used [173–175]. When graphene serves as a high-conductivity filler in the composite materials, it is more likely to have few-layer graphene than a single-layer one [10]. Within a cluster, van der Waals forces usually exist between the LD materials. These interaction forces will couple the dynamics of individual pieces together and modify the thermal transport properties. Here we provide a review of the clustering effect on the thermal conductivity of LD materials.

Layer effect on 2D materials

For layered materials, the most common form of a cluster is to form a few-layer stack, as shown in Figure 13a. Because of the interlayer coupling, the thermal properties of few-layer 2D materials can be different from those of a single-layer one. The availability of high-quality few-layer graphene makes it possible to experimentally explore the layer effects on graphene. Using micro-Raman spectroscopy, Ghosh et al. measured the thermal conductivity of few-layer graphene (two, three, four, and eight layers) as well as high-quality graphite [96]. They found that the thermal conductivity of few-layer graphene decreases with increasing number of layers. This is in contrast to thin-film materials, in which the thermal conductivity should increase with the film thickness due to weaker phonon–boundary scattering [96]. By calculating the phonon dispersion of few-layer graphene from first principles and accounting for the allowed Umklapp scattering process, they provided two reasons for their observation [96]. First, due to the interlayer coupling, the dispersion curves of some low-frequency acoustic modes are flattened and hence their contributions to thermal conductivity are reduced. Second, the available states for three-phonon Umklapp scattering in the high-frequency range increase with an increase of the number of layers [96]. For example, the available phonon states for scattering in bilayer graphene are four times that in single-layer graphene in the high-frequency range [96]. Later, Lindsay et al. [97] also found that the thermal conductivity of few-layer graphene is lower than that of single-layer graphene. This layer thickness dependence of thermal conductivity is quite different for supported [54] and encased [176]
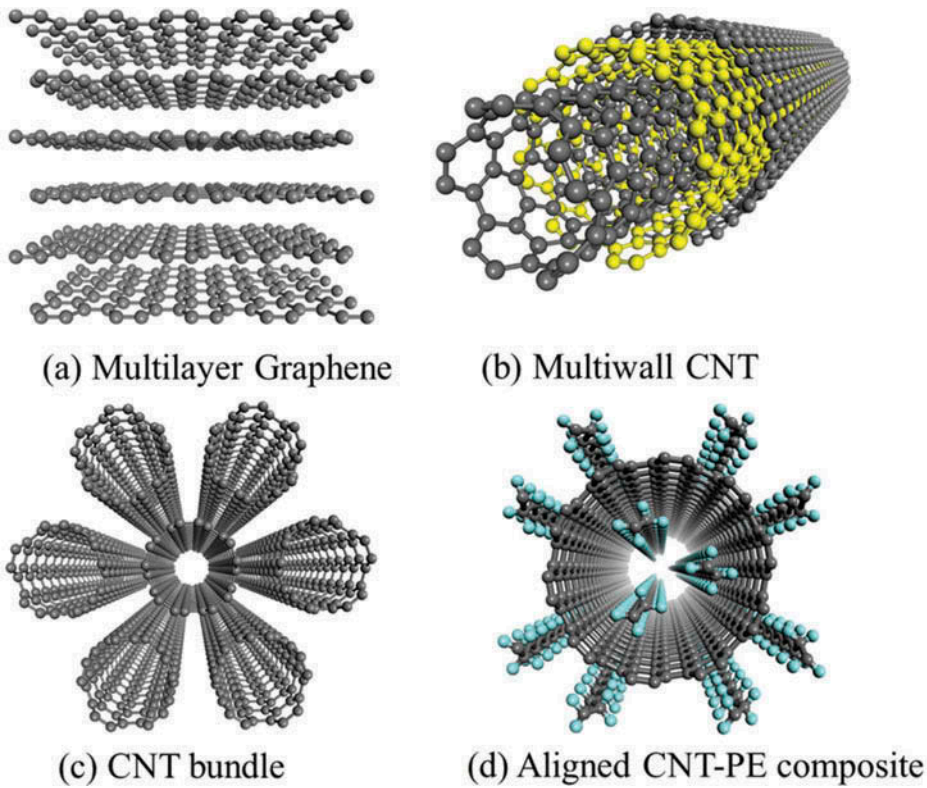
Figure 13. Clustering of low-dimensional materials: (a) few-layer graphene, (b) multiwalled CNTs, (c) CNT bundles, and (d) aligned CNT-PE composite.

few-layer graphene. For supported few-layer graphene, measurements carried out by Sadeghi et al. [54] indicate that the in-plane thermal conductivity of few-layer graphene increases with increasing number of layers, as discussed previously, and this phenomenon is explained by the long phonon mean free paths in the cross-plane direction and the partially diffuse scattering of phonons at the few-layer graphene/a-SiO$_2$ interface. A similar increase in thermal conductivity with increasing number of layers is also found in encased few-layer graphene by a heat spreader measurement [176]. The authors adopted a phenom-enological model that the coupling interaction at the few-layer graphene/a-SiO$_2$ interface only affects the thermal properties of the outermost graphene layers to explain the experimental data [176]. Through NEMD simulations, Wei et al. also found that the interaction in multilayer graphene could impede the phonon transport along the in-plane direction in multilayer graphene films [177]. Similar to the interaction between graphene and the substrate, the interlayer interaction between graphene layers could also be covalent bonded (sp^3-bonded) [178, 179]. Guo et al. [180] investigated the effect of interlayer sp^3 bonding on the thermal transport in bilayer graphene through NEMD simulations. Compared to the case of bilayer graphene with van der Waals interaction, they found that the formation of sp^3 bonding can induce additional thermal conductivity reduction, and the amount of reduction is largely dependent on the sp^3 bonding ratio and its distributions [180]. In fact, bilayer graphene could be stacked in different sequences, including AA-stacked and AB-stacked [181, 182]. Liu et al. investigated the stacking of bilayer graphene on its thermal conductivity through NEMD simulations [183]. They found that the AA-stacking bilayer graphene has slightly higher thermal conductivity than the AB stacking bilayer graphene and attributed this difference to the fact that AB-stacked bilayer graphene has a strong interlayer coupling strength [183].

In addition, h-BN has a lattice structure very similar to that of graphene. Therefore, the layer effect on h-BN is almost identical to that on graphene. For example, Lindsay and Broido also investigated the thermal transport in few-layer h-BN and found that the coupling between neighboring layers in multilayer h-BN can also break the phonon scattering selection rule found in single-layer BN [87]. Gao et al. [184] studied the effect of interlayer covalent bonding on the thermal conductivity of bilayer h-BN through NEMD simulations. The results show that the thermal conductivity is sensitive to the distribution of the covalent bonding [184], which is similar to the case of graphene [180].

Other 2D materials, such as phosphorene, MoS_2, and Bi_2Te_3 QL have different atomic structures compared to graphene and h-BN. The layer effects on these materials are different from the case of pure 2D material. For phosphorene, NEMD simulations show that the in-plane thermal conductivity is insensitive to the layer number, which is different from graphene, for which the interlayer interactions strongly influence the thermal transport [185]. The weak thickness dependence of thermal conductivity of black phosphorus thin film is also found through four-probe measurement and first principles calculation [93]. For MoS_2, the layer thickness-dependent thermal conductivities are studied through first principles calculations [95]. The authors found that the thermal conductivity of MoS_2 decreases monotonically with an increase in layer number. For naturally occurring trilayer MoS_2, the thermal conductivity reduced to 71% of the single-layer MoS_2, which is very close to the bulk value [95]. They found that the change in dispersion curve due to the interlayer coupling plays an important role in the reduction. For example, in trilayer MoS_2, the change in the dispersion curve itself can lead to a 15% reduction in thermal conductivity compared to the single-layer MoS_2, and the change in the anharmonicity (i.e., the third-order force constants and phonon scattering rate) contributes the rest of the reduction. Qiu and Ruan [186] investigated the layer effect in Bi_2Te_3 QL through EMD simulations. The found that the in-plane thermal conductivity of Bi_2Te_3 QLs first decreases and then increases with an increase in layer number. The thermal conductivity reaches a minimum value of 1.1 W/mK for three layers, in comparison to 1.6 W/mK in single Bi_2Te_3 QL and 1.3 W/mK in bulk Bi_2Te_3. The initial decrease in thermal conductivity with an increase in layers is attributed to interlayer coupling-induced phonon scattering, and the further increase in thermal conductivity with an increase in number of layers is attributed to the diminishing of classical boundary scattering effect. The existence of diffusive boundary scattering in Bi_2Te_3 thin film is also experimentally observed with thickness down to 9 QLs [43, 187]. The diminishing of classical size due to the van der Waals coupling is also observed experimentally in boron nanoribbons (the thickness of the ribbons is ~20 nm) by Yang et al. [67]. They found that the thermal conductivity of a double ribbon coupled by van der Waals interaction is higher than that of a single ribbon and attributed this to the fact that phonon specular scattering occurred at the van der Waals interface between two ribbons but diffusive scattering occurred at the free surfaces of ribbons [67, 188]. We summarize the layer effects on different 2D materials in Table 3.

CNT bundle

Unlike 2D materials, CNTs tend to form a multiwalled structure or bundled structure due to the van der Waals interaction, as shown in Figures 13b and 13c. Hsu et al. measured the thermal

Table 3. Summary of layer effects on 2D materials.

Material	Method	Layer effect	Reference
Graphene	Raman measurement	Decrease from 2,800 to 1,300 as the number of layers increases from two to four	[96]
Graphene	BTE	Decreases monotonically with increasing layer number	[97]
Bi_2Te_3 QL	Green-Kubo	First a decrease and then an increase with layer number	[186]
h-BN	BTE	Decrease with the increase of layer number and converge to the bulk value within a few layers	[87]
MoS_2	BTE	Monotonically reduce when its thickness increases from one layer to three layers	[95]
Phosphorene	NEMD	Insensitive to the layer number	[185]

conductivity of single-walled CNT bundles using a Raman spectroscopy method [189]. In their samples, there were four to five CNTs in each bundle and the length of the bundle was on the order of 10 μm [189]. They found that room temperature thermal conductivities of single-walled CNT bundles range from 118 to 683 W/mK, which is lower than that of individual single-walled CNTs [31]. Intertube coupling, defects, and thermal contact resistance between the nanotubes are believed to be responsible for the low thermal conductivity [189]. The thermal conductivity of multiwalled CNT bundles was also measured by Volkov et al. using a self-heating 3ω method [170]. The length of the bundle is also around 10 μm, but the number of tubes in the bundle could be up to 100. They found that the thermal conductivity of bundles decreases with the number of tubes in the bundle, and the lowest case has about 100 tubes and the thermal conductivity is 150 W/mK [170]. In some other research works, the thermal conductivity of a multiwalled carbon nanotube bundle was characterized by a Raman-based electrical method or optical method and the values are on the order of 10 W/mK [190, 191], which is far below the values obtained in other experiments. The CNT bundle quality could be the reason for the large difference in different measurements. Similar low thermal conductivity has been observed in buckypaper composed of randomly distributed carbon nanotubes [192].

Because the thermal resistance of bulk LD material (either bundle or fiber) is from the internal thermal contact resistance between these composition materials, it is feasible to modulate the thermal transport of bulk materials by adjusting the internal thermal contact resistance. As mentioned in the previous section, the strain effect can be used to manipulate intrinsic thermal conductivity of LD materials and can be used to change the contact resistance between them when forming bulk materials, which can be realized through external forces such as mechanical stretching or compression. Yue et al. investigated the thermal transport of aligned carbon nanotube fibers and accomplished thermal manipulation through mechanical stretching [193]. The results show that thermal conductivity of well-aligned carbon nanotube fibers can be improved by 30% with elongation less than 5%, as shown in Figure 14. In addition, sample temperature has a significant effect on thermal properties.

Aligned polymers

Although 1D polymer chains such as PE chains have high thermal conductivity, the polymer fibers and arrays are easier for applications and more important. How the interchain van der Waals (VDW) interactions will affect the phonon transport is unknown.

This is not easy to predict because the interchain interactions introduce not only the new phonon modes to carry heat but also phonon–phonon scatterings to deduct the transport. Henry et al. [194] investigated why the thermal conductivity of polyethylene decreases in the process from 1D to 3D transition using EMD simulations. They found that the transition from 1D (single chain) to 2D (single lattice plane) is sharper than the transition from 2D to 3D (array). The authors concluded that opening up new routes for phonon–phonon scattering is dominant while introducing more modes for propagating heat is negligible compared to the longitudinal acoustic phonons. Cao et al. [171, 195] experimentally measured the thermal properties of PE nanowire arrays. The thermal conductivities of nanowire arrays with diameters of 200 and 100 nm reach 20.5 and 26.5 W/mK, respectively. The discrepancy is a consequence of more orientated structures due to the smaller diameter of the nanowires.

In addition, the interchain interactions can make confinements on the movement of atoms, which will result in crystal-like vibrations and increase the thermal conductivity. By NEMD, Liao et al. [196] reported that the thermal conductivity of aligned CNT-PE composites is as high as 99.5 W/mK with 320 nm in length. More interesting, it will diverge when the length keeps increasing. The high thermal conductivity is attributed to the high thermal conductivity of CNT, the alignment, and the confinements on vibrations due to VDW interactions between PE and CNT. Yu et al. [197] proposed a bulk structure, the crosswise paved polyethylene laminate (CPPEL). Similar to the multilayer
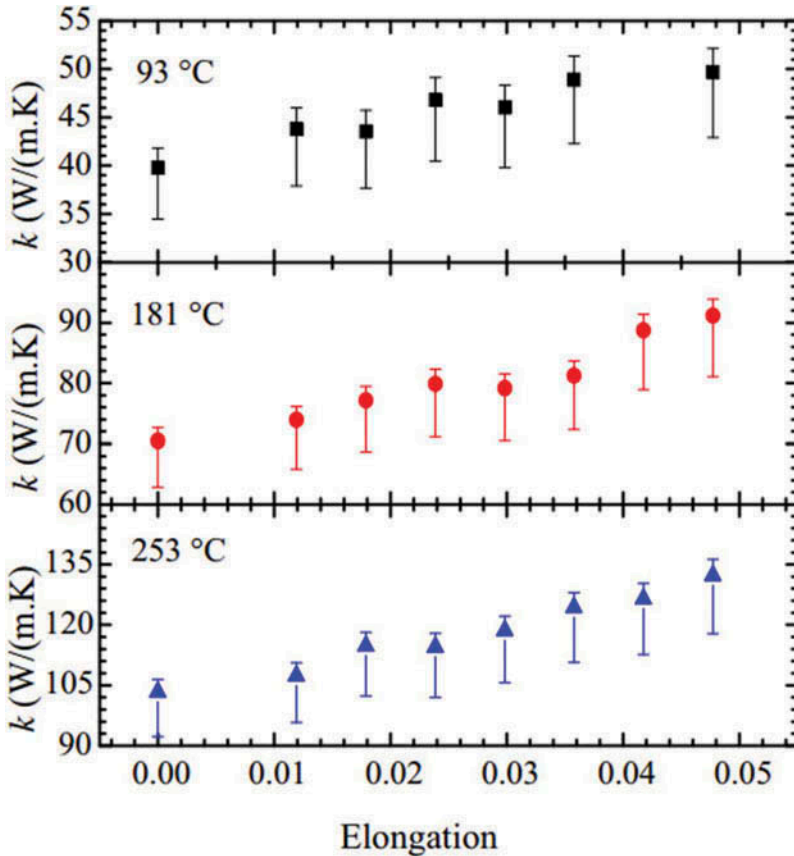
Figure 14. Thermal conductivities of multiwalled CNT fibers at different elongations and temperatures. Adapted from Yue et al. [193] with permission.

structure of graphite, the aligned chains are paved layer by layer and the aligned directions are crosswise for two adjacent layers. The thermal conductivity of CPPEL is calculated as 181 W/mK along two in-plane directions by EMD. In addition to the enhanced value, CPPEL has high thermal conductivity along two in-plane directions instead of one. The authors attributed the enhanced thermal conductivity to the crosswise layout, which weakens the wiggles and confines the segmental rotations by interchain VDW interactions. The analysis suggested the crystal-like atomic vibrations in CPPEL.

3D architectures of graphene

Although graphene possesses excellent thermal transport properties, the 2D structure limits its application and it becomes a challenge in integrating the material from 2D to 3D with proper thermal characteristics. Current bulk materials composed of graphene flakes include graphene foam [198–200], graphene fiber [201], and graphene aerogel [202]. The purpose of such an engineering attempt is either for thermal interface materials (TIM) material with better heat dissipation performance or for thermal insulation material to prevent heat transfer because the bulk materials differ greatly from the thermal characteristics of graphene. For example, Pettes et al. measured the thermal conductivity of graphene foam from 0.26 to 1.7 W/mK [198], which is a few orders of magnitude lower than the thermal conductivity of suspended monolayer graphene. Upon annealing at 3000°C, the 3D architectures exhibit

an increase in solid thermal conductivity to nearly 900 W/mK at room temperature [203]. Lin et al. characterized the thermal diffusivity of graphene foam using a transient electrothermal technique. The effective thermal diffusivity of the GF samples was measured as 3.86–7.40 × 10^{-5} m^2/s [199]. Li et al. investigated the temperature effect on the thermal properties of graphene foams. Thermal conductivity and thermal diffusivity increased from ~0.3 to 1.5 W/mK and ~4 × 10^{-5} to ~2 × 10^{-4} m^2/s, respectively, with temperature from 310 to 440 K [200]. A wide range of measurement values in these works stems from the difference in graphene sample quality, layer number, flake size, and chemical compositions.

Graphene aerogel is another 3D architecture of graphene that is fabricated from graphene oxide using chemical reduction methods. Because graphene flakes have been oxidized, their thermal properties have been reduced significantly. Fan et al. reported that the thermal conductivities of graphene aerogels are measured to be 0.12–0.36 W/mK [202]. Xie et al. reported the thermal characterization result of an extremely light graphene aerogel about two times heavier than air [204]. It was found that its thermal conductivity (4.7 × 10^{-3} to 5.9 × 10^{-3} W/mK) at room temperature is about 80% lower than that of air (0.0257 W/mK at 20°C). At low temperatures, its thermal conductivity reaches a lower level of 2 × 10^{-4} to 4 × 10^{-4} W/mK [204]. Therefore, it can be used as an excellent thermal insulation material. From another point of view, because the 3D architecture of graphene exhibits different thermal characteristics, its property can be well modulated by changing composite material, adjusting the flake size of graphene, and oxidation treatment for different thermal application needs.

Distinct effects

Due to the structure specificity of LD materials, some distinct and brand new effects have been found recently, such as bending, folding, pinching, and twisting effects, which are not applicable for bulk materials. For example, the bending effect of carbon nanotubes can modify their mechanical and thermal properties [205]. Based on the folding effect of graphene, the instantaneously adjustable thermal resistor was proposed as a brand new thermal device [206]. The pinching effect of nanowires can reduce the thermal conductivity and enhance thermoelectric performance [207]. The twisting effect can control the thermal properties [121]. All of these distinct effects show that LD materials have potential applications in a broad field.

Bending effect

As shown in Figure 15a, bending is usually imposed by rotating the two ridged ends to a target angle, which leads to a buckling kink and corresponding bending angle. Thus, the original cylindrical shape of the nanotube is highly distorted, which results in modification of the mechanical and thermal properties of the bent CNT around the kinks. The buckling kinks hamper phonon transport along the buckled nanotube. For bent CNTs with lengths less than the phonon mean free path, both ballistic and diffusive phonon transport coexist [205].

Volkov et al. [208] revealed a strong dependence (close to inverse proportionality) of the thermal conductance of the buckling kink on the buckling angle through NEMD simulations. The value of the buckling kink conductance ranges from 40 to 10 GWm^{-2}K^{-1} as the buckling angle changes from 20° to 110°. Using NEMD, Ma et al. [205] uncovered that the phonon propagation is significantly affected by the occurrence of localized structural buckling at short length, whereas heat transport becomes insensitive to the buckling deformations as the length becomes comparable to the phonon mean free path.

Pinching effect

In 2009, Tian et al. [209] synthesized a new type of building block–kinked silicon nanowire (KSiNW). Stimulated by KSiNWs, several groups have synthesized kinks in other nanowires, such as In$_2$O$_3$ multikinked nanowires [210], kinked germanium nanowires [211], germanium silicon axial heterostructure with kinks [212], and kinked ZnO nanowires [213]. Jiang et al. [207] performed MD

simulations to investigate the reduction in thermal conductivity by kinks in silicon nanowires and found that the reduction percentage can be as high as 70% at room temperature. Furthermore, Ma et al. accomplished an even lower thermal conductivity by constructing nano cross junctions with SiNWs [214]. By calculating phonon polarization vectors, two mechanisms are found to be responsible for the reduced thermal conductivity: (1) the interchanging effect between the longitudinal and transverse phonon modes and (2) the pinching effect; that is, a new type of localization for the twisting and transverse phonon modes in the kinked silicon nanowires.

Folding effect

In 2008, folded graphene had a different electronic structure compared to monolayer graphene [216], which leaves room to manipulate the properties of graphene derivatives, or folding. Recently, the multiply folded graphene has been realized experimentally [217, 218]. Therefore, there is a need for review of thermal management by folding.

Based on folded graphene nanoribbons (GNRs, shown in Figure 15c and the nonequilibrium Green's function method, Ouyang et al. [215] reported a thermal conductance modulator by varying the folding angle, layer distance, and center region length, which can modulate the thermal conductance along the folding direction with a tuning range up to 40% of the conductance of unfolded nanoribbons. Through NEMD simulations, Yang et al. [219] found that the thermal conductivity along the folding direction of flat GNRs can be modulated by different folds and by changing interlayer couplings. Through the analysis of transmission, the authors revealed that the reduction in thermal conductivity is due to scattering of low-frequency phonons by the folds.

Using the nonequilibrium Green's function method, Li et al. [220] illustrated that the curvature effect results in a slight decrease in the thermal conductance of GNRs. The analysis shows that the curvature effect reduces the phonon transmission coefficient at $600 \text{ cm}^{-1} < \omega < 800 \text{ cm}^{-1}$. By NEMD simulations, Zhang et al. [221] found an abnormal phenomenon that the thermal conductivity of armchair GNRs perpendicular to the folding direction increases dramatically as the folding angle increases, and that of zigzag GNRs decreases more quickly.
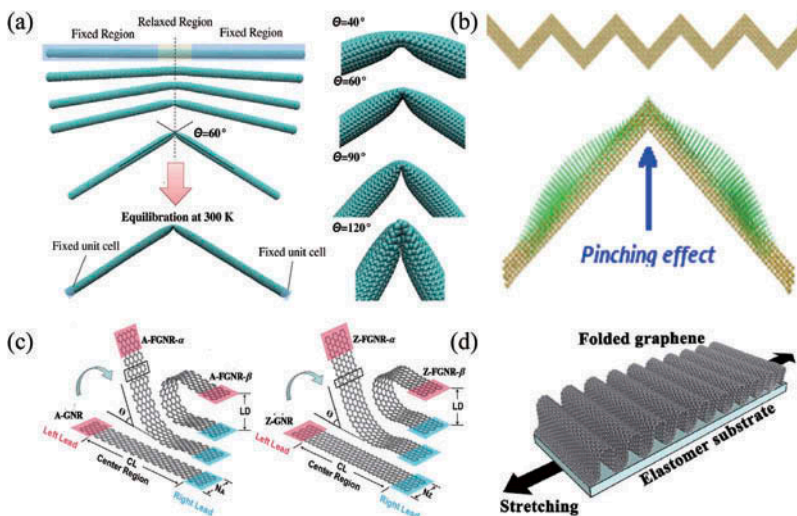

Figure 15. (a) Bending effect of single-walled carbon nanotube. (b) Pinching effect of silicon nanowire. (c) Folding effect of graphene nanoribbon. (d) Schematic of adjustable thermal resistor base on large-area graphene. Parts (a)–(d) are adapted from Volkov et al. [208], Jiang et al. [207], Ouyang et al. [215], and Song et al. [206] with permission.

Song et al. [206] proposed an instantaneously adjustable thermal resistor based on the folding effects of large-area graphene, as shown in Figure 15d. The thermal resistivity shows a linear dependence on the characteristic size, $1/L$ and $1/L_{plane}$ (L and L_{plane} denote the overall length and the distance between two folds). Through the analysis of power spectral density, this phenomenon stems from the size effect and folding scattering by the folds.

Twisting effect

Twisting provides another approach to control the thermal properties of low-dimensional materials, as shown in Figure 16. Using NEMD simulations, Xu and Buehler [120] applied a torsional strain of $n2\pi/L$ on CNTs, where n is an integer and L is the length of the simulation box along the tube axis. They found that CNTs preserve their cylindrical shape and the thermal conductivity changes only by around 1% at small twist strain. When the strain continues to increase, CNTs start to buckle in the cross section, which results in a 20% drop in the thermal conductivity at twist strain of ~0.04. By reverse NEMD, Wei et al. [121] reported that the thermal conductivity of GNR decreases with an increase in twist angle. However, zigzag GNRs with open edges do not buckle. Instead, they form a tube-like structure at a torsional angle of 2π and reduce thermal conductivity by approximately 10%. When the torsional angle increases to 3π, the structure turns tube-like with unevenly distributed diameters and the thermal conductivity drops significantly by about 40% due to strong phonon interface scattering. Moreover, the phonon spectra of twisted GNRs become closer to that of CNTs as the torsional angle increases.

Summary and outlook

To date, there have been numerous investigations on the external perturbation effects on the thermal transport of low-dimensional materials. We have reviewed the effects of commonly existing perturbations, including mechanical strain, supporting on a substrate, forming a cluster, and some distinct effects on the thermal properties of common LD materials. Some key observations are summarized below:

Strain

Compressive strain usually leads to deformation of the lattice structure of LD materials, which will induce additional phonon scattering and lower the thermal conductivity. The effect of tensile strain could be different in different materials. For graphene, the tensile strain effect remains controversial.
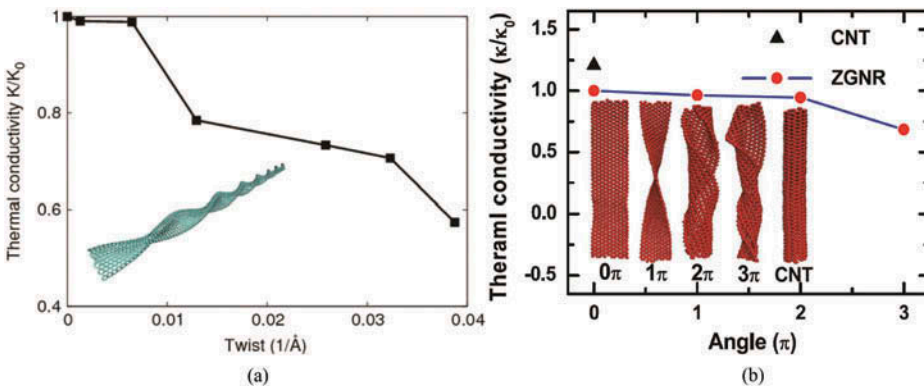

Figure 16. Twisting effect of (a) carbon nanotube and (b) graphene nanoribbon. Parts (a) and (b) are adapted from Xu and Buehler [120] and Wei et al. [121] with permission.

Depending on different numerical methods and conditions (sample size, types of strain, etc.), the thermal conductivity could be diverging, unchanged, or increasing with strain. For nonplanar 2D materials like silicene and phosphorene, tensile strain makes the structure more planar, and the lattice thermal conductivity of LD materials can increase significantly with the applied tensile strain. For some other materials like BN and MoS_2, the thermal conductivity usually first increases and then decreases with tensile strain. For 1D materials, the tensile strain also has different effects on thermal transport. The thermal conductivity decreases for CNTs due to the enhanced anharmonicity. On the contrary, the tensile strain can reduce phonon scattering and increase the thermal conductivity of PE chains. In nanostructures, the regularity of strain effects on phonon scattering is not obvious. Both a full understanding of theory and systematic experimental study are need.

Substrate

Interaction with a substrate will usually suppress the thermal transport in LD materials, but the extent is largely dependent on the choice of substrates (e.g., crystalline or amorphous, lattice mismatch, surface morphology, etc.) and the coupling strength at the interface. These studies provide useful guidance for the choice of appropriate substrates for desired applications. For multilayer graphene, a large layer thickness is required to recover its bulk thermal conductivity value when supported on a substrate. Some studies also show that the particular substrate and coupling strength could lead to an enhancement in the thermal conductivity of the supported materials. In these cases, the dispersion curve of the supported material may be quite different from the freestanding one. However, the underlying mechanism for the unusual enhancement in the thermal conductivity remains unclear and is worth exploring further. On the other hand, there are few studies on the substrate effect on the thermal properties of polymers. The substrate effect from nonflat substrate surfaces is also less investigated.

Clustering

For 2D materials like graphene and BN, their thermal conductivity will show a clear decay with an increased number of layers and then saturate to bulk values at few atomic layers, whereas for some nonplanar and few-atomic-layer materials like phosphorene and Bi_2Te_3 QL, the thermal conductivity is relatively insensitive to the number of layers. For 1D materials it will form a bundle structure. The effective thermal conductivity of the bundle is typically less than the individual value, which is mainly due to the suppression of long mean free path modes. However, some recent simulation results show that the existence of van der Waals force could enhance the thermal performance of nanoribbons and polymer chains. Therefore, more theoretical and experimental works are needed to explore the effect of the van der Waals force on nanostructures.

Distinct effects

Due to the structure specificity of LD materials, we discussed some distinct effects in nanostructures; that is, bending, pinching, folding, and twisting, all of which lead to more phonon scattering and a reduction in thermal conductivity. These effects open new routes for the modulation of thermal conductivity and the design of thermal devices, such as the instantaneously adjustable thermal resistor based on the folding effects of graphene. However, most of the current studies are theoretical, and further experimental research should be conducted to push the application of these effects. On the other hand, it is worth exploring distinct nano-effects to enhance heat transfer, which have wide potential applications in electronics and optoelectronics.

From the existing literature, it is still difficult to reach universal conclusions on how the external factors can affect the thermal transport properties. These external perturbations have complicated effects on thermal properties of the LD materials from different aspects, including lattice structure, harmonic properties, and anharmonic properties. These factors are often coupled together, making

the relative importance of each factor difficult to identify. The overall effect on the thermal conductivity is largely dependent on the atomic structure of the LD materials and the extent of the perturbation. We notice that, in many existing publications, many types of environmental perturbations are simply regarded as boundary and the modification of thermal conductivity is attributed to phonon–boundary scattering. However, this concept is adopted from the classical size effect of bulk materials, and it is not applicable for the case when the perturbation is applied to the finite dimension of LD materials. We also notice that for the substrate effect and clustering, the nature of the interaction is still not clear. For theoretical investigations, it is usually assumed to be van der Waals forces but experimental verification is lacking. Another point worth mentioning is that most of the investigations are focused on the lattice thermal transport, though charge carrier thermal transport could also be important in LD materials.

In the near future, related research still needs to be carried out for individual materials and particular types of perturbation. In addition, most of the current works are based on numerical simulations, including MD-based methods and first principles–based anharmonic lattice dynamics (ALD). Depending on simulation details, the conclusions can be different in different works. More careful numerical investigations should be carried out to resolve the controversies. Experimental investigations for precisely quantitative analysis are still quite limited or even missing, which is also a great challenge.

Acknowledgments

Funding

References

1. A.H. Castro Neto, F. Guinea, N.M.R. Peres, K.S. Novoselov, and A.K. Geim, The Electronic Properties of Graphene, *Reviews of Modern Physics*, Vol. 81, pp. 109–162, 2009.
2. L. Li, Y. Yu, G.J. Ye, Q. Ge, X. Ou, H. Wu, D. Feng, X.H. Chen, and Y. Zhang, Black Phosphorus Field-Effect Transistors, *Nature Nanotechnology*, Vol. 9, pp. 372–377, 2014.
3. L. Tao, E. Cinquanta, D. Chiappe, C. Grazianetti, M. Fanciulli, M. Dubey, A. Molle, and D. Akinwande, Silicene Field-Effect Transistors Operating at Room Temperature, *Nature Nanotechnology*, Vol. 10, pp. 227–231, 2015.
4. H. Shi, H. Pan, Y.-W. Zhang, and B. I. Yakobson, Quasiparticle Band Structures and Optical Properties of Strained Monolayer MoS2 and WS2, *Physical Review B*, Vol. 87, pp. 155304, 2013.
5. L. Matthes, O. Pulci, and F. Bechstedt, Optical Properties of Two-Dimensional Honeycomb Crystals Graphene, Silicene, Germanene, and Tinene from First Principles, *New Journal of Physics*, Vol. 16, pp. 105007, 2014.
6. H. Bao, B. Duvvuri, M. Lou, and X. Ruan, Effects of Randomness and Inclination on the Optical Properties of Multi-Walled Carbon Nanotube Arrays, *Journal of Quantitative Spectroscopy and Radiative Transfer*, Vol. 132, pp. 22–27, 2014.
7. S. Berber, Y.-K. Kwon, and D. Tomanek, Unusually High Thermal Conductivity of Carbon Nanotubes, *Physical Review Letters*, Vol. 84, pp. 4613–4616, 2000.
8. A.A. Balandin, S. Ghosh, W. Bao, I. Calizo, D. Teweldebrhan, F. Miao, and C.N. Lau, Superior Thermal Conductivity of Single-Layer Graphene, *Nano Letters*, Vol. 8, pp. 902–907, 2008.
9. A.A. Balandin, Thermal Properties of Graphene and Nanostructured Carbon Materials, *Nature Materials*, Vol. 10, pp. 569–581, 2011.
10. K.M.F. Shahil and A.A. Balandin, Thermal Properties of Graphene and Multilayer Graphene: Applications in Thermal Interface Materials, *Solid State Communications*, Vol. 152, pp. 1331–1340, 2012.
11. H. Bao, C. Shao, S. Luo, and M. Hu, Enhancement of Interfacial Thermal Transport by Carbon Nanotube–Graphene Junction, *Journal of Applied Physics*, Vol. 115, pp. 53524, 2014.

12. T. Kuilla, S. Bhadra, D. Yao, N.H. Kim, S. Bose, andJ.H. Lee, Recent Advances in Graphene Based Polymer Composites, *Progress in Polymer Science*, Vol. 35, pp. 1350–1375, 2010.

13. X. Huang, X. Qi, F. Boey, and H. Zhang, Graphene-Based Composites, *Chemical Society Reviews*, Vol. 41, pp. 666–686, 2012.

14. S. Rakheja, V. Kumar, and A. Naeemi, Evaluation of the Potential Performance of Graphene Nanoribbons as On-Chip Interconnects, *Proceedings of the IEEE*, Vol. 101, pp. 1740–1765, 2013.

15. A. Henry and G. Chen, High Thermal Conductivity of Single Polyethylene Chains Using Molecular Dynamics Simulations, *Physical Review Letters*, Vol. 101, pp. 235502, 2008.

16. S. Shen, A. Henry, J. Tong, R. Zheng, and G. Chen, Polyethylene Nanofibres with Very High Thermal Conductivities, *Nature Nanotechnology*, Vol. 5, pp. 251–255, 2010.

17. G. Fiori, F. Bonaccorso, G. Iannaccone, T. Palacios, D. Neumaier, A. Seabaugh, S.K. Banerjee, and L. Colombo, Electronics Based on Two-Dimensional Materials, *Nature Nanotechnology*, Vol. 9, pp. 768–779, 2014.

18. B. Radisavljevic, A. Radenovic, J. Brivio, V. Giacometti, and A. Kis, Single-Layer MoS2 Transistors, *Nature Nanotechnology*, Vol. 6, pp. 147–150, 2011.

19. C.R. Dean, A.F. Young, I. Meric, C. Lee, L. Wang, S. Sorgenfrei, K. Watanabe, T. Taniguchi, P. Kim, K.L. Shepard, and J. Hone, Boron Nitride Substrates for High-Quality Graphene Electronics, *Nature Nanotechnology*, Vol. 5, pp. 722–726, 2010.

20. D. Teweldebrhan, V. Goyal, and A.A. Balandin, Exfoliation and Characterization of Bismuth Telluride Atomic Quintuples and Quasi-Two-Dimensional Crystals, *Nano Letters*, Vol. 10, pp. 1209–1218, 2010.

21. D. Teweldebrhan, V. Goyal, M. Rahman, and A.A. Balandin, Atomically-Thin Crystalline Films and Ribbons of Bismuth Telluride, *Applied Physics Letters*, Vol. 96, pp. 53107, 2010.

22. A.M. Marconnet, M.A. Panzer, and K.E. Goodson, Thermal Conduction Phenomena in Carbon Nanotubes and Related Nanostructured Materials, *Reviews of Modern Physics*, Vol. 85, pp. 1295–1326, 2013.

23. J. Peng, G. Zhang, and B. Li, Thermal Management in MoS2 Based Integrated Device Using Near-Field Radiation, *Applied Physics Letters*, Vol. 107, pp. 133108, 2015.

24. R. Yan, J.R. Simpson, S. Bertolazzi, J. Brivio, M. Watson, X. Wu, A. Kis, T. Luo, A.R. Hight Walker, and H.G. Xing, Thermal Conductivity of Monolayer Molybdenum Disulfide Obtained from Temperature-Dependent Raman Spectroscopy, *ACS Nano*, Vol. 8, pp. 986–993, 2014.

25. A.I. Hochbaum, R. Chen, R.D. Delgado, W. Liang, E.C. Garnett, M. Najarian, A. Majumdar, and P. Yang, Enhanced Thermoelectric Performance of Rough Silicon Nanowires, *Nature*, Vol. 451, pp. 163–167, 2008.

26. D.L. Nika and A.A. Balandin, Two-Dimensional Phonon Transport in Graphene, *Journal of Physics: Condensed Matter*, Vol. 24, pp. 233203, 2012.

27. Y. Wang, A.K. Vallabhaneni, B. Qiu, and X. Ruan, Two-Dimensional Thermal Transport in Graphene: A Review of Numerical Modeling Studies, *Nanoscale and Microscale Thermophysical Engineering*, Vol. 18, pp. 155–182, 2014.

28. N. Yang, X. Xu, G. Zhang, and B. Li, Thermal Transport in Nanostructures, *AIP Advances*, Vol. 2, pp. 41410, 2012.

29. X. Gu and R. Yang, Phonon Transport and Thermal Conductivity in Two-Dimensional Materials, *arXiv:1509.07762 [cond-mat]*, 2015.

30. D. Donadio, *Simulation of dimensionality effects in thermal transport,* in *Thermal Transport in Low Dimensions*, pp. 275–304, Springer, 2016.

31. M. Fujii, X. Zhang, H. Xie, H. Ago, K. Takahashi, T. Ikuta, H. Abe, and T. Shimizu, Measuring the Thermal Conductivity of a Single Carbon Nanotube, *Physical Review Letters*, Vol. 95, pp. 65502, 2005.

32. T.-Y. Choi, D. Poulikakos, J. Tharian, and U. Sennhauser, Measurement of the Thermal Conductivity of Individual Carbon Nanotubes by the Four-Point Three-ω Method, *Nano Letters*, Vol. 6, pp. 1589–1593, 2006.

33. P. Kim, L. Shi, A. Majumdar, and P. McEuen, Thermal Transport Measurements of Individual Multiwalled Nanotubes, *Physical Review Letters*, Vol. 87, pp. 215502–215505, 2001.

34. C. Faugeras, B. Faugeras, M. Orlita, M. Potemski, R.R. Nair, and A.K. Geim, Thermal Conductivity of Graphene in Corbino Membrane Geometry, *ACS Nano*, Vol. 4, pp. 1889–1892, 2010.

35. J.-U. Lee, D. Yoon, H. Kim, S. W. Lee, and H. Cheong, Thermal Conductivity of Suspended Pristine Graphene Measured by Raman Spectroscopy, *Physical Review B*, Vol. 83, pp. 81419, 2011.

36. W. Cai, A.L. Moore, Y. Zhu, X. Li, S. Chen, L. Shi, and R.S. Ruoff, Thermal Transport in Suspended and Supported Monolayer Graphene Grown by Chemical Vapor Deposition, *Nano Letters*, Vol. 10, pp. 1645–1651, 2010.

37. N. Mingo and D.A. Broido, Length Dependence of Carbon Nanotube Thermal Conductivity and the "Problem of Long Waves," *Nano Letters*, Vol. 5, pp. 1221–1225, 2005.

38. N. Bonini, J. Garg, and N. Marzari, Acoustic Phonon Lifetimes and Thermal Transport in Free-Standing and Strained Graphene, *Nano Letters*, Vol. 12, pp. 2673–2678, 2012.

39. L.F.C. Pereira and D. Donadio, Divergence of the Thermal Conductivity in Uniaxially Strained Graphene, *Physical Review B*, Vol. 87, pp. 125424, 2013.

40. Y. Shen, G. Xie, X. Wei, K. Zhang, M. Tang, J. Zhong, G. Zhang, and Y.-W. Zhang, Size and Boundary Scattering Controlled Contribution of Spectral Phonons to the Thermal Conductivity in Graphene Ribbons, *Journal of Applied Physics*, Vol. 115, pp. 63507, 2014.

41. N. Yang, G. Zhang, and B. Li, Ultralow Thermal Conductivity of Isotope-Doped Silicon Nanowires, *Nano Letters*, Vol. 8, pp. 276–280, 2008.

42. X. Wu, N. Yang, and T. Luo, Unusual Isotope Effect on Thermal Transport of Single Layer Molybdenum Disulphide, *Applied Physics Letters*, Vol. 107, pp. 191907, 2015.

43. M.T. Pettes, J. Kim, W. Wu, K.C. Bustillo, and L. Shi, Thermoelectric Transport in Surface- and Antimony-Doped Bismuth Telluride Nanoplates, *APL Materials*, Vol. 4, pp. 104810, 2016.

44. S.-K. Chien, Y.-T. Yang, and C.-K. Chen, Influence of Hydrogen Functionalization on Thermal Conductivity of Graphene: Nonequilibrium Molecular Dynamics Simulations, *Applied Physics Letters*, Vol. 98, pp. 33107, 2011.

45. P.-C. Ma, N A. Siddiqui, G. Marom, and J.-K. Kim, Dispersion and Functionalization of Carbon Nanotubes for Polymer-Based Nanocomposites: A Review, *Composites Part A: Applied Science and Manufacturing*, Vol. 41, pp. 1345–1367, 2010.

46. H. Wang, T. Maiyalagan, and X. Wang, Review on Recent Progress in Nitrogen-Doped Graphene: Synthesis, Characterization, and Its Potential Applications, *ACS Catalysis*, Vol. 2, pp. 781–794, 2012.

47. S. Kwon, M.C. Wingert, J. Zheng, J. Xiang, and R. Chen, Thermal transport in Si and Ge Nanostructures in the "Confinement" Regime, *Nanoscale*, Vol. 8, pp. 13155–13167, 2016.

48. R. Roldán, A. Castellanos-Gomez, E. Cappelluti, and F. Guinea, Strain Engineering in Semiconducting Two-Dimensional Crystals, *Journal of Physics: Condensed Matter*, Vol. 27, pp. 313201, 2015.

49. Z. Liu, M. Amani, S. Najmaei, Q. Xu, X. Zou, W. Zhou, T. Yu, C. Qiu, A.G. Birdwell, F.J. Crowne, R. Vajtai, B.I. Yakobson, Z. Xia, M. Dubey, P.M. Ajayan, and J. Lou, Strain and Structure Heterogeneity in MoS2 Atomic Layers Grown by Chemical Vapour Deposition, *Nature Communications*, Vol. 5, pp. 5246, 2014.

50. X. Wang, K. Tantiwanichapan, J.W. Christopher, R. Paiella, and A. K. Swan, Uniaxial Strain Redistribution in Corrugated Graphene: Clamping, Sliding, Friction, and 2D Band Splitting, *Nano Letters*, Vol. 15, pp. 5969–5975, 2015.

51. A.A. Mitioglu, K. Galkowski, A. Surrente, L. Klopotowski, D. Dumcenco, A. Kis, D.K. Maude, and P. Plochocka, Magnetoexcitons in Large Area CVD-Grown Monolayer MoS2 and MoSe2 on Sapphire, *Physical Review B*, Vol. 93, pp. 165412, 2016.

52. J. Liu and R. Yang, Tuning the Thermal Conductivity of Polymers with Mechanical Strains, *Physical Review B*, Vol. 81, pp. 174122, 2010.

53. M. Hu, X. Zhang, and D. Poulikakos, Anomalous Thermal Response of Silicene to Uniaxial Stretching, *Physical Review B*, Vol. 87, pp. 195417, 2013.

54. M.M. Sadeghi, I. Jo, and L. Shi, Phonon–Interface Scattering in Multilayer Graphene on an Amorphous Support, *PNAS*, Vol. 110, pp. 16321–16326, 2013.

55. T. Sun, J. Wang, and W. Kang, Van der Waals Interaction–Tuned Heat Transfer in Nanostructures, *Nanoscale*, Vol. 5, pp. 128–133, 2013.

56. K.D. Parrish, A. Jain, J.M. Larkin, W.A. Saidi, and A.J.H. McGaughey, Origins of Thermal Conductivity Changes in Strained Crystals, *Physical Review B*, Vol. 90, pp. 235201, 2014.

57. X. Li, K. Maute, M.L. Dunn, and R. Yang, Strain Effects on the Thermal Conductivity of Nanostructures, *Physical Review B*, Vol. 81, pp. 245318, 2010.

58. Y. Kuang, L. Lindsay, and B. Huang, Unusual Enhancement in Intrinsic Thermal Conductivity of Multilayer Graphene by Tensile Strains, *Nano Letters*, Vol. 15, pp. 6121–6127, 2015.

59. T. Zhu and E. Ertekin, Resolving Anomalous Strain Effects on Two-Dimensional Phonon Flows: The Cases of Graphene, Boron Nitride, and Planar Superlattices, *Physical Review B*, Vol. 91, pp. 205429, 2015.

60. H. Xie, T. Ouyang, E. Germaneau, G. Qin, M. Hu, and H. Bao, Large Tunability of Lattice Thermal Conductivity of Monolayer Silicene via Mechanical Strain, *Physical Review B*, Vol. 93, pp. 75404, 2016.

61. J.H. Seol, I. Jo, A.L. Moore, L. Lindsay, Z.H. Aitken, M.T. Pettes, X. Li, Z. Yao, R. Huang, D. Broido, N. Mingo, R.S. Ruoff, and L. Shi, Two-Dimensional Phonon Transport in Supported Graphene, *Science*, Vol. 328, pp. 213–216, 2010.

62. Z.-Y. Ong, E. Pop, and J. Shiomi, Reduction of Phonon Lifetimes and Thermal Conductivity of a Carbon Nanotube on Amorphous Silica, *Physical Review B*, Vol. 84, pp. 165418, 2011.

63. B. Qiu and X. Ruan, Reduction of Spectral Phonon Relaxation Times from Suspended to Supported Graphene, *Applied Physics Letters*, Vol. 100, pp. 193101, 2012.

64. X. Zhang, H. Bao, and M. Hu, Bilateral Substrate Effect on the Thermal Conductivity of Two-Dimensional Silicon, *Nanoscale*, Vol. 7, pp. 6014–6022, 2015.

65. J., Hone, M. Whitney, C. Piskoti, and A. Zettl, Thermal Conductivity of Single-Walled Carbon Nanotubes, *Physical Review B*, Vol. 59, pp. R2514, 1999.

66. X.H. Yan, Y. Xiao, and Z.M. Li, Effects of Intertube Coupling and Tube Chirality on Thermal Transport of Carbon Nanotubes, *Journal of Applied Physics*, Vol. 99, pp. 124305, 2006.

67. J. Yang, Y. Yang, S.W. Waltermire, X. Wu, H. Zhang, T. Gutu, Y. Jiang, Y. Chen, A.A. Zinn, R. Prasher, T.T. Xu, and D. Li, Enhanced and Switchable Nanoscale Thermal Conduction Due to Van der Waals Interfaces, *Nature Nanotechnology*, Vol. 7, pp. 91–95, 2012.

68. W. Chen, J. Yang, Z. Wei, C. Liu, K. Bi, D. Xu, D. Li, and Y. Chen, Effects of Interfacial Roughness on Phonon Transport in Bilayer Silicon Thin Films, *Physical Review B*, Vol. 92, pp. 134113, 2015.

69. D. Ma, H. Ding, X. Wang, N. Yang, and X. Zhang, The Unexpected Thermal Conductivity from Graphene Disk, Carbon Nanocone to Carbon Nanotube, *International Journal of Heat and Mass Transfer*, Vol. 108, pp. 940–944, 2017.

70. J.C. Meyer, A. K. Geim, M.I. Katsnelson, K.S. Novoselov, T.J. Booth, and S. Roth, The Structure of Suspended Graphene Sheets, *Nature*, Vol. 446, pp. 60–63, 2007.

71. Z.F. Ren, Z.P. Huang, J.W. Xu, J.H. Wang, P. Bush, M.P. Siegal, and P.N. Provencio, Synthesis of Large Arrays of Well-Aligned Carbon Nanotubes on Glass, *Science*, Vol. 282, pp. 1105–1107, 1998.

72. L. Song, L. Ci, H. Lu, P.B. Sorokin, C. Jin, J. Ni, A.G. Kvashnin, D.G. Kvashnin, J. Lou, B.I. Yakobson, and P.M. Ajayan, Large Scale Growth and Characterization of Atomic Hexagonal Boron Nitride Layers, *Nano Letters*, Vol. 10, pp. 3209–3215, 2010.

73. Y. Stehle, H.M. Meyer, R.R. Unocic, M. Kidder, G. Polizos, P.G. Datskos, R. Jackson, S.N. Smirnov, and I.V. Vlassiouk, Synthesis of Hexagonal Boron Nitride Monolayer: Control of Nucleation and Crystal Morphology, *Chemistry of Materials*, Vol. 27, pp. 8041–8047, 2015.

74. P. Vogt, P. De Padova, C. Quaresima, J. Avila, E. Frantzeskakis, M.C. Asensio, A. Resta, B. Ealet, and G. Le Lay, Silicene: Compelling Experimental Evidence for Graphene-Like Two-Dimensional Silicon, *Physical Review Letters*, Vol. 108, pp. 155501, 2012.

75. H. Xie, M. Hu, and H. Bao, Thermal Conductivity of Silicene from First-Principles, *Applied Physics Letters*, Vol. 104, pp. 131906, 2014.

76. H. Liu, A.T. Neal, Z. Zhu, Z. Luo, X. Xu, D. Tomanek, and P.D. Ye, Phosphorene: An Unexplored 2D Semiconductor with a High Hole Mobility, *ACS Nano*, Vol. 8, pp. 4033–4041, 2014.

77. Q. Wei and X. Peng, Superior Mechanical Flexibility of Phosphorene and Few-Layer Black Phosphorus, *Applied Physics Letters*, Vol. 104, pp. 251915, 2014.

78. Y.-H. Lee, X.-Q. Zhang, W. Zhang, M.-T. Chang, C.-T. Lin, K.-D. Chang, Y.-C. Yu, J.T.-W. Wang, C.-S. Chang, L.-J. Li, and T.-W. Lin, Synthesis of Large-Area MoS2 Atomic Layers with Chemical Vapor Deposition, *Advanced Materials*, Vol. 24, pp. 2320–2325, 2012.

79. Q. Peng and S. De, Outstanding Mechanical Properties of Monolayer MoS2 and Its Application in Elastic Energy Storage, *Physical Chemistry Chemical Physics*, Vol. 15, pp. 19427–19437, 2013.

80. J.M. Ziman, *Electrons and Phonons: The Theory of Transport Phenomena in Solids*, Oxford University Press, Clarendon, Oxford, 1960.

81. L. Lindsay, D.A. Broido, and N. Mingo, Flexural Phonons and Thermal Transport in Graphene, *Physical Review B*, Vol. 82, pp. 115427, 2010.

82. A. Jain and A.J.H. McGaughey, Thermal Conductivity of Compound Semiconductors: Interplay of Mass Density and Acoustic–Optical Phonon Frequency Gap, *Journal of Applied Physics*, Vol. 116, pp. 73503, 2014.

83. E. Mariani and F. von Oppen, Flexural Phonons in Free-Standing Graphene, *Physical Review Letters*, Vol. 100, pp. 76801, 2008.

84. H. Zabel, Phonons in Layered Compounds, *Journal of Physics: Condensed Matter*, Vol. 13, pp. 7679–7690, 2001.

85. L.D. Landau and E.M. Lifshitz, *Theory of Elasticity, Vol. 7, Course of Theoretical Physics*, 3rd ed., Pergamon Press, 1986.

86. R. Al-Jishi and G. Dresselhaus, Lattice-Dynamical Model for Graphite, *Physical Review B*, Vol. 26, pp. 4514–4522, 1982.

87. L. Lindsay and D.A. Broido, Theory of Thermal Transport in Multilayer Hexagonal Boron Nitride and Nanotubes, *Physical Review B*, Vol. 85, pp. 35436, 2012.

88. X. Fan, W.T. Zheng, J.-L. Kuo, and D.J. Singh, Structural Stability of Single-Layer MoS2 under Large Strain, *Journal of Physics: Condensed Matter*, Vol. 27, pp. 105401, 2015.

89. A. Molina-Sánchez and L. Wirtz, Phonons in Single-Layer and Few-Layer MoS2 and WS2, *Physical Review B*, Vol. 84, pp. 155413, 2011.

90. X. Zhang, et al. Thermal Conductivity of Silicene Calculated Using an Optimized Stillinger-Weber Potential, *Physical Review B*, Vol. 89, pp. 54310, 2014.

91. L. Lindsay, First Principles Peierls-Boltzmann Phonon Thermal Transport: A Topical Review, *Nanoscale and Microscale Thermophysical Engineering*, Vol. 20, pp. 67–84, 2016.

92. J. Carrete, W. Li, L. Lindsay, D.A. Broido, L.J. Gallego, and N. Mingo, Physically Founded Phonon Dispersions of Few-Layer Materials and the Case of Borophene, *Materials Research Letters*, Vol. 4, pp. 204–211, 2016.

93. B. Smith, B. Vermeersch, J. Carrete, E. Ou, J. Kim, N. Mingo, D. Akinwande, and L. Shi, Temperature and Thickness Dependences of the Anisotropic In-Plane Thermal Conductivity of Black Phosphorus, *Advanced Materials*, pp. 1603756, 1603761.

94. J. Liu, G.-M. Choi, and D.G. Cahill, Measurement of the Anisotropic Thermal Conductivity of Molybdenum Disulfide by the Time-Resolved Magneto-Optic Kerr Effect, *Journal of Applied Physics*, Vol. 116, pp. 233107, 2014.

95. X. Gu, B. Li, and R. Yang, Layer Thickness-Dependent Phonon Properties and Thermal Conductivity of MoS2, *Journal of Applied Physics*, Vol. 119, pp. 85106, 2016.

96. S. Ghosh, W. Bao, D.L. Nika, S. Subrina, E.P. Pokatilov, C.N. Lau, and A.A. Balandin, Dimensional Crossover of Thermal Transport in Few-Layer Graphene, *Nature Materials*, Vol. 9, pp. 555–558, 2010.

97. L. Lindsay, D.A. Broido, and N. Mingo, Flexural Phonons and Thermal Transport in Multilayer Graphene and Graphite, *Physical Review B*, Vol. 83, pp. 235428, 2011.

98. N. Mingo, Calculation of Si Nanowire Thermal Conductivity Using Complete Phonon Dispersion Relations, *Physical Review B*, Vol. 68, pp. 113308, 2003.

99. H. Bao, X.L. Ruan, and M. Kaviany, Theory of the Broadening of Vibrational Spectra Induced by Lowered Symmetry in Yttria Nanostructures, *Physical Review B*, Vol. 78, pp. 125417, 2008.

100. R.H. Baughman, A.A. Zakhidov, and W.A. de Heer, Carbon Nanotubes—The Route Toward Applications, *Science*, Vol. 297, pp. 787–792, 2002.

101. S.Y. Zhou, G.-H. Gweon, A.V. Fedorov, P.N. First, W.A. de Heer, D.-H. Lee, F. Guinea, A.H. Castro Neto, and A. Lanzara, Substrate-Induced Bandgap Opening in Epitaxial Graphene, *Nature Materials*, Vol. 6, pp. 770–775, 2007.

102. Z.H. Ni, T. Yu, Y.H. Lu, Y.Y. Wang, Y.P. Feng, and Z.X. Shen, Uniaxial Strain on Graphene: Raman Spectroscopy Study and Band-Gap Opening, *ACS Nano*, Vol. 2, pp. 2301–2305, 2008.

103. H.H. Babaei, A.J. McGaughey, and C.E. Wilmer, Effect of Pore Size and Shape on the Thermal Conductivity of Metal-Organic Frameworks, *Chemical Science*, Vol. 8, pp. 583–589, 2017.

104. C. Shao and H. Bao, A Molecular Dynamics Investigation of Heat Transfer across a Disordered Thin Film, *International Journal of Heat and Mass Transfer*, Vol. 85, pp. 33–40, 2015.

105. J.E. Turney, E.S. Landry, A.J.H. McGaughey, and C.H. Amon, Predicting Phonon Properties and Thermal Conductivity from Anharmonic Lattice Dynamics Calculations and Molecular Dynamics Simulations, *Physical Review B*, Vol. 79, pp. 64301, 2009.

106. T. Feng and X. Ruan, Prediction of Spectral Phonon Mean Free Path and Thermal Conductivity with Applications to Thermoelectrics and Thermal Management: A Review, *Journal of Nanomaterials*, Vol. 2014, pp. e206370, 2014.

107. J.A. Thomas, J.E. Turney, R.M. Iutzi, C.H. Amon, and A.J.H. McGaughey, Predicting Phonon Dispersion Relations and Lifetimes from the Spectral Energy Density, *Physical Review B*, Vol. 81, pp. 81411, 2010.

108. A. McGaughey, Predicting Phonon Properties from Equilibrium Molecular Dynamics Simulations, *Annual Reviews of Heat Transfer*, Vol. 17, pp. 49–87, 2014.

109. C. Shao and H. Bao, Thermal Transport in Bismuth Telluride Quintuple Layer: Mode-Resolved Phonon Properties and Substrate Effects, *Scientific Reports*, Vol. 6, pp. 27492, 2016.

110. D.A. Broido, A. Ward, and N. Mingo, Lattice Thermal Conductivity of Silicon from Empirical Interatomic Potentials, *Physical Review B*, Vol. 72, pp. 14308, 2005.

111. G. Fugallo, M. Lazzeri, L. Paulatto, and F. Mauri, Ab initio Variational Approach for Evaluating Lattice Thermal Conductivity, *Physical Review B*, Vol. 88, pp. 45430, 2013.

112. T. Feng and X. Ruan, Quantum Mechanical Prediction of Four-Phonon Scattering Rates and Reduced Thermal Conductivity of Solids, *Physical Review B*, Vol. 93, pp. 45202, 2016.

113. Y. Yue, J. Zhang, and X. Wang, Micro/Nanoscale Spatial Resolution Temperature Probing for the Interfacial Thermal Characterization of Epitaxial Graphene on 4H-SiC, *Small*, Vol. 7, pp. 3324–3333, 2011.

114. L. Shi, D. Li, C. Yu, W. Jang, D. Kim, Z. Yao, P. Kim, and A. Majumdar, Measuring Thermal and Thermoelectric Properties of One-Dimensional Nanostructures Using a Microfabricated Device, *Journal of Heat Transfer*, Vol. 125, pp. 881–888, 2003.

115. G. Plechinger, A. Castellanos-Gomez, M. Buscema, H.S.J. van der Zant, G.A. Steele, A. Kuc, T. Heine, C. Schuller, and T. Korn, Control of Biaxial Strain in Single-Layer Molybdenite Using Local Thermal Expansion of the Substrate, *2D Materials*, Vol. 2, pp. 15006, 2015.

116. P.R. Shaina, L. George, V. Yadav, and M. Jaiswal, Estimating the Thermal Expansion Coefficient of Graphene: The Role of Graphene–Substrate Interactions, *Journal of Physics: Condensed Matter*, Vol. 28, pp. 85301, 2016.

117. C. Si, Z. Sun, and F. Liu, Strain Engineering of Graphene: A Review, *Nanoscale*, Vol. 8, pp. 3207–3217, 2016.

118. X. Peng, Q. Wei, and A. Copple, Strain-Engineered Direct–Indirect Band Gap Transition and Its Mechanism in Two-Dimensional Phosphorene, *Physical Review B*, Vol. 90, pp. 85402, 2014.

119. L. Zhu, T. Zhang, Z. Sun, J. Li, G. Chen, and S.A. Yang, Thermal Conductivity of Biaxial-Strained MoS2: Sensitive Strain Dependence and Size-Dependent Reduction Rate, *Nanotechnology*, Vol. 26, pp. 465707, 2015.

120. Z. Xu and M.J. Buehler, Strain Controlled Thermomutability of Single-Walled Carbon Nanotubes, *Nanotechnology*, Vol. 20, pp. 185701, 2009.

121. N. Wei, L. Xu, H.-Q. Wang, and J.-C. Zheng, Strain Engineering of Thermal Conductivity in Graphene Sheets and Nanoribbons: A Demonstration of Magic Flexibility, *Nanotechnology*, Vol. 22, pp. 105705, 2011.

122. F. Ma, H.B. Zheng, Y.J. Sun, D. Yang, K.W. Xu, and P.K. Chu, Strain Effect on Lattice Vibration, Heat Capacity, and Thermal Conductivity of Graphene, *Applied Physics Letters*, Vol. 101, pp. 111904, 2012.
123. Y.K. Koh, M.-H. Bae, D.G. Cahill, and E. Pop, Heat Conduction across Monolayer and Few-Layer Graphenes, *Nano Letters*, Vol. 10, pp. 4363–4368, 2010.
124. M. Gill-Comeau, and L.J. Lewis, Heat Conductivity in Graphene and Related Materials: A Time-Domain Modal Analysis, *Physical Review B*, Vol. 92, pp. 195404, 2015.
125. S.J. Chae, F. Güneş, K.K. Kim, E.S. Kim, G.H. Han, S.M. Kim, H.-J. Shin, S.-M. Yoon, J.-Y. Choi, M.H. Park, C.W. Yang, D. Pribat, and Y.H. Lee, Synthesis of Large-Area Graphene Layers on Poly-Nickel Substrate by Chemical Vapor Deposition: Wrinkle Formation, *Advanced Materials*, Vol. 21, pp. 2328–2333, 2009.
126. W. Bao, F. Miao, Z. Chen, H. Zhang, W. Jang, C. Dames, and C.N. Lau, Controlled Ripple Texturing of Suspended Graphene and Ultrathin Graphite Membranes, *Nature Nanotechnology*, Vol. 4, pp. 562–566, 2009.
127. K. Xu, P. Cao, and J.R. Heath, Scanning Tunneling Microscopy Characterization of the Electrical Properties of Wrinkles in Exfoliated Graphene Monolayers, *Nano Letters*, Vol. 9, pp. 4446–4451, 2009.
128. J. Zang, S. Ryu, N. Pugno, Q. Wang, Q. Tu, M.J. Buehler, and X. Zhao, Multifunctionality and Control of the Crumpling and Unfolding of Large-Area Graphene, *Nature Materials*, Vol. 12, pp. 321–325, 2013.
129. S. Chen, Q. Li, Q. Zhang, Y. Qu, H. Ji, R.S. Ruoff, and W. Cai, Thermal Conductivity Measurements of Suspended Graphene with and without Wrinkles by Micro-Raman Mapping, *Nanotechnology*, Vol. 23, pp. 365701, 2012.
130. K.L. Grosse, V.E. Dorgan, D. Estrada, J.D. Wood, I. Vlassiouk, G. Eres, J.W. Lyding, W.P. King, and E. Pop, Direct Observation of Resistive Heating at Graphene Wrinkles and Grain Boundaries, *Applied Physics Letters*, Vol. 105, pp. 143109, 2014.
131. L. Lindsay, W. Li, J. Carrete, N. Mingo, D.A. Broido, and T.L. Reinecke, Phonon Thermal Transport in Strained and Unstrained Graphene from First Principles, *Physical Review B*, Vol. 89, pp. 155426, 2014.
132. G. Fugallo, A. Cepellotti, L. Paulatto, M. Lazzeri, N. Marzari, and F. Mauri, Thermal Conductivity of Graphene and Graphite: Collective Excitations and Mean Free Paths, *Nano Letters*, Vol. 14, pp. 6109–6114, 2014.
133. B. Amorim, A. Cortijo, F. de Juan, A.G. Grushin, F. Guinea, A. Gutiérrez-Rubio, H. Ochoa, V. Parente, R. Roldn, P. San-Jose, J. Schiefele, M. Sturla, and M.A.H. Vozmediano, Novel Effects of Strains in Graphene and Other Two Dimensional Materials, *Physics Reports*, Vol. 617, pp. 1–54, 2016.
134. Y.Y. Zhang, Q.X. Pei, X.Q. He, and Y.-W. Mai, A Molecular Dynamics Simulation Study on Thermal Conductivity of Functionalized Bilayer Graphene Sheet, *Chemical Physics Letters*, Vol. 622, pp. 104–108, 2015.
135. T. Zhang and T. Luo, Morphology-Influenced Thermal Conductivity of Polyethylene Single Chains and Crystalline Fibers, *Journal of Applied Physics*, Vol. 112, pp. 94304, 2012.
136. Q.-X. Pei, Y.-W. Zhang, Z.-D. Sha, and V.B. Shenoy, Tuning the Thermal Conductivity of Silicene with Tensile Strain and Isotopic Doping: A Molecular Dynamics Study, *Journal of Applied Physics*, Vol. 114, pp. 33526, 2013.
137. X. Gu and R. Yang, First-Principles Prediction of Phononic Thermal Conductivity of Silicene: A Comparison with Graphene, *Journal of Applied Physics*, Vol. 117, pp. 25102, 2015.
138. Y.D. Kuang, L. Lindsay, S.Q. Shi, and G.P. Zheng, Tensile Strains Give Rise to Strong Size Effects for Thermal Conductivities of Silicene, Germanene and Stanene, *Nanoscale*, Vol. 8, pp. 3760–3767, 2016.
139. Z. Ding, Q.-X. Pei, J.-W. Jiang, and Y.-W. Zhang, Manipulating the Thermal Conductivity of Monolayer MoS2 via Lattice Defect and Strain Engineering, *Journal of Physical Chemistry C*, Vol. 119, pp. 16358–16365, 2015.
140. Z.-X. Guo, J.W. Ding, and X.-G. Gong, Substrate Effects on the Thermal Conductivity of Epitaxial Graphene Nanoribbons, *Physical Review B*, Vol. 85, pp. 235429, 2012.
141. J. Zhang, Y. Wang, and X. Wang, Rough Contact Is Not Always Bad for Interfacial Energy Coupling, *Nanoscale*, Vol. 5, pp. 11598, 2013.
142. Y. Yue, J. Zhang, X. Tang, S. Xu, and X. Wang, Thermal Transport across Atomic-Layer Material Interfaces, *Nanotechnology Reviews*, Vol. 4, pp. 533–555, 2015.
143. G. Le Lay, 2D Materials: Silicene Transistors, *Nature Nanotechnology*, Vol. 10, pp. 202–203, 2015.
144. X. Li, W. Cai, J. An, S. Kim, J. Nah, D. Yang, R. Piner, A. Velamakanni, I. Jung, E. Tutuc, S.K. Banerjee, L. Colombo, and R.S. Ruoff, Large-Area Synthesis of High-Quality and Uniform Graphene Films on Copper Foils, *Science*, Vol. 324, pp. 1312–1314, 2009.
145. K.V. Emtsev, F. Speck, T. Seyller, L. Ley, and J.D. Riley, Interaction, Growth, and Ordering of Epitaxial Graphene on SiC{0001} Surfaces: A Comparative Photoelectron Spectroscopy Study, *Physical Review B*, Vol. 77, pp. 155303, 2008.
146. C.-L. Lin, R. Arafune, K. Kawahara, N. Tsukahara, E. Minamitani, Y. Kim, N. Takagi, and M. Kawai, Structure of Silicene Grown on Ag(111), *Applied Physics Express*, Vol. 5, pp. 45802–45804, 2012.
147. F. Bonaccorso, Z. Sun, T. Hasan, and A.C. Ferrari, Graphene Photonics and Optoelectronics, *Nature Photonics*, Vol. 4, pp. 611–622, 2010.
148. A.V. Babichev, S.A. Rykov, M. Tchernycheva, A.N. Smirnov, V.Y. Davydov, Y.A. Kumzerov, and V.Y. Butko, Influence of Substrate Microstructure on the Transport Properties of CVD–Graphene, *ACS Applied Materials & Interfaces*, Vol. 8, pp. 240–246, 2016.

149. R. Quhe, Y. Yuan, J. Zheng, Y. Wang, Z. Ni, J. Shi, D. Yu, J. Yang, and J. Lu, Does the Dirac Cone Exist in Silicene on Metal Substrates? *Scientific Reports*, Vol. 4, pp. 5476–5483, 2014.

150. P. Sutter, J.T. Sadowski, and E.A. Sutter, Chemistry under Cover: Tuning Metal–Graphene Interaction by Reactive Intercalation, *Journal of the American Chemical Society*, Vol. 132, pp. 8175–8179, 2010.

151. R. Friedlein, A. Fleurence, J.T. Sadowski, and Y. Yamada-Takamura, Tuning of Silicene–Substrate Interactions with Potassium Adsorption, *Applied Physics Letters*, Vol. 102, pp. 221603, 2013.

152. S. Das, D. Lahiri, A. Agarwal, and W. Choi, Interfacial Bonding Characteristics between Graphene and Dielectric Substrates, *Nanotechnology*, Vol. 25, pp. 45707, 2014.

153. A.V. Savin, B. Hu, and Y.S. Kivshar, Thermal Conductivity of Single-Walled Carbon Nanotubes, *Physical Review B*, Vol. 80, pp. 195423, 2009.

154. A.V. Savin, Y.S. Kivshar, and B. Hu, Effect of Substrate on Thermal Conductivity of Single-Walled Carbon Nanotubes, *EPL*, Vol. 88, pp. 26004, 2009.

155. Z.-Y. Ong and E. Pop, Effect of Substrate Modes on Thermal Transport in Supported Graphene, *Physical Review B*, Vol. 84, pp. 75471, 2011.

156. B. Amorim and F. Guinea, Flexural Mode of Graphene on a Substrate, *Physical Review B*, Vol. 88, pp. 115418, 2013.

157. H. Sevinçli and M. Brandbyge, Phonon Scattering in Graphene over Substrate Steps, *Applied Physics Letters*, Vol. 105, pp. 153108, 2014.

158. H. Mi, S. Mikael, C.-C. Liu, J.-H. Seo, G. Gui, A.L. Ma, P.F. Nealey, and Z. Ma, Creating Periodic Local Strain in Monolayer Graphene with Nanopillars Patterned by Self-Assembled Block Copolymer, *Applied Physics Letters*, Vol. 107, pp. 143107, 2015.

159. S. Neogi, J.S. Reparaz, L.F.C. Pereira, B. Graczykowski, M.R. Wagner, M. Sledzinska, A. Shchepetov, M. Prunnila, J. Ahopelto, C.M. Sotomayor-Torres, and D. Donadio, Tuning Thermal Transport in Ultrathin Silicon Membranes by Surface Nanoscale Engineering, *ACS Nano*, Vol. 9, pp. 3820–3828, 2015.

160. W.A. de Heer, C. Berger, X. Wu, P.N. First, E.H. Conrad, X. Li, T. Li, M. Sprinkle, J. Hass, M.L. Sadowski, M. Potemski, and G. Martinez, Epitaxial Graphene, *Solid State Communications*, Vol. 143, pp. 92–100, 2007.

161. F. Hiebel, P. Mallet, F. Varchon, L. Magaud, and J.-Y. Veuillen, Graphene–Substrate Interaction on 6H-SiC, 0001-): A Scanning Tunneling Microscopy Study, *Physical Review B*, Vol. 78, pp. 153412, 2008.

162. K.-X. Chen, X.-M. Wang, D.-C. Mo, and S.-S. Lyu, Substrate Effect on Thermal Transport Properties of Graphene on SiC(0 0 0 1) Surface, *Chemical Physics Letters*, Vol. 618, pp. 231–235, 2015.

163. Z. Wei, J. Yang, K. Bi, and Y. Chen, Mode Dependent Lattice Thermal Conductivity of Single Layer Graphene, *Journal of Applied Physics*, Vol. 116, pp. 153503, 2014.

164. J. Chen, G. Zhang, and B. Li, Substrate Coupling Suppresses Size Dependence of Thermal Conductivity in Supported Graphene, *Nanoscale*, Vol. 5, pp. 532–536, 2013.

165. J. Liu, T. Wang, S. Xu, P. Yuan, X. Xu, and X. Wang, Thermal Conductivity of Giant Mono- to Few-Layered CVD Graphene Supported on an Organic Substrate, *Nanoscale*, Vol. 8, pp. 10298–10309, 2016.

166. W. Zhao, W. Chen, Y. Yue, and S. Wu, In-situ Two-Step Raman Thermometry for Thermal Characterization of Monolayer Graphene Interface Material, *Applied Thermal Engineering*, Vol. 113, pp. 481–489, 2017.

167. Z. Wang, T. Feng, and X. Ruan, Thermal Conductivity and Spectral Phonon Properties of Freestanding and Supported Silicene, *Journal of Applied Physics*, Vol. 117, pp. 84317, 2015.

168. B. Qiu, Y. Wang, Q. Zhao, and X. Ruan, The Effects of Diameter and Chirality on the Thermal Transport in Free-Standing and Supported Carbon-Nanotubes, *Applied Physics Letters*, Vol. 100, pp. 233105, 2012.

169. A.M. Pantano, D. Parks, and M.C. Boyce, Mechanics of Deformation of Single- and Multi-Wall Carbon Nanotubes, *Journal of the Mechanics and Physics of Solids*, Vol. 52, pp. 789–821, 2004.

170. A.N. Volkov, R.N. Salaway, and L.V. Zhigilei, Atomistic Simulations, Mesoscopic Modeling, and Theoretical Analysis of Thermal Conductivity of Bundles Composed of Carbon Nanotubes, *Journal of Applied Physics*, Vol. 114, pp. 104301, 2013.

171. B.-Y. Cao, J. Kong, Y. Xu, K.-L. Yung, and A. Cai, Polymer Nanowire Arrays with High Thermal Conductivity and Superhydrophobicity Fabricated by a Nano-Molding Technique, *Heat Transfer Engineering*, Vol. 34, pp. 131–139, 2013.

172. J.J. Yoo, K. Balakrishnan, J. Huang, V. Meunier, B.G. Sumpter, A. Srivastava, M. Conway, A.L.M. Reddy, J. Yu, R. Vajtai, and P.M. Ajayan, Ultrathin Planar Graphene Supercapacitors, *Nano Letters*, Vol. 11, pp. 1423–1427, 2011.

173. J. Xu and T.S. Fisher, Enhancement of Thermal Interface Materials with Carbon Nanotube Arrays, *International Journal of Heat and Mass Transfer*, Vol. 49, pp. 1658–1666, 2006.

174. B.A. Cola, J. Xu, C. Cheng, X. Xu, T.S. Fisher, and H. Hu, Photoacoustic Characterization of Carbon Nanotube Array Thermal Interfaces, *Journal of Applied Physics*, Vol. 101, pp. 54313, 2007.

175. S. Kaur, N. Raravikar, B.A. Helms, R. Prasher, and D.F. Ogletree, Enhanced Thermal Transport at Covalently Functionalized Carbon Nanotube Array Interfaces, *Nature Communications*, Vol. 5, pp. 3082–3089, 2014.

176. W. Jang, Z. Chen, W. Bao, C.N. Lau, and C. Dames, Thickness-Dependent Thermal Conductivity of Encased Graphene and Ultrathin Graphite, *Nano Letters*, Vol. 10, pp. 3909–3913, 2010.

177. Z. Wei, Z. Ni, K. Bi, M. Chen, and Y. Chen, In-Plane Lattice Thermal Conductivities of Multilayer Graphene Films, *Carbon*, Vol. 49, pp. 2653–2658, 2011.
178. J. Kanasaki, E. Inami, K. Tanimura, H. Ohnishi, and K. Nasu, Formation of sp^3-Bonded Carbon Nanostructures by Femtosecond Laser Excitation of Graphite, *Physical Review Letters*, Vol. 102, pp. 87402, 2009.
179. M.K. Zalalutdinov, J.T. Robinson, C.E. Junkermeier, J.C. Culbertson, T.L. Reinecke, R. Stine, P.E. Sheehan, B.H. Houston, and E.S. Snow, Engineering Graphene Mechanical Systems, *Nano Letters*, Vol. 12, pp. 4212–4218, 2012.
180. T. Guo, Z.-D. Sha, X. Liu, G. Zhang, T. Guo, Q.-X. Pei, and Y.-W. Zhang, Tuning the Thermal Conductivity of Multi-Layer Graphene with Interlayer Bonding and Tensile Strain, *Applied Physics A*, Vol. 120, pp. 1275–1281, 2015.
181. S.-J. Tsai, Y.-H. Chiu, Y.-H. Ho, and M.-F. Lin, Gate-Voltage-Dependent Landau Levels in AA-Stacked Bilayer Graphene, *Chemical Physics Letters*, Vol. 550, pp. 104–110, 2012.
182. Y.-H. Ho, Y.-H. Chiu, D.-H. Lin, C.-P. Chang, and M.-F. Lin, Magneto-Optical Selection Rules in Bilayer Bernal Graphene, *ACS Nano*, Vol. 4, pp. 1465–1472, 2010.
183. Y. Liu, H. Yang, N. Liao, and P. Yang, Investigation on Thermal Conductivity of Bilayer Graphene Nanoribbons, *RSC Advances*, Vol. 4, pp. 54474–54479, 2014.
184. Y. Gao, X. Zhang, Y. Jing, and M. Hu, The Unexpected Non-Monotonic Inter-Layer Bonding Dependence of the Thermal Conductivity of Bilayered Boron Nitride, *Nanoscale*, Vol. 7, pp. 7143–7150, 2015.
185. Y.-Y. Zhang, Q.-X. Pei, J.-W. Jiang, N. Wei, and Y.-W. Zhang, Thermal Conductivities of Single- and Multi-Layer Phosphorene: A Molecular Dynamics Study, *Nanoscale*, Vol. 8, pp. 483–491, 2016.
186. B. Qiu and X. Ruan, Thermal Conductivity Prediction and Analysis of Few-Quintuple Bi2Te3 Thin Films: A Molecular Dynamics Study, *Applied Physics Letters*, Vol. 97, pp. 183107, 2010.
187. M.T. Pettes, J. Maassen, I. Jo, M.S. Lundstrom, and L. Shi, Effects of Surface Band Bending and Scattering on Thermoelectric Transport in Suspended Bismuth Telluride Nanoplates, *Nano Letters*, Vol. 13, pp. 5316–5322, 2013.
188. D. Li and A.J.H. McGaughey, Phonon Dynamics at Surfaces and Interfaces and Its Implications in Energy Transport in Nanostructured Materials—An Opinion Paper, *Nanoscale and Microscale Thermophysical Engineering*, Vol. 19, pp. 166–182, 2015.
189. I.-K. Hsu, M.T. Pettes, A. Bushmaker, M. Aykol, L. Shi, and S.B. Cronin, Optical Absorption and Thermal Transport of Individual Suspended Carbon Nanotube Bundles, *Nano Letters*, Vol. 9, pp. 590–594, 2009.
190. Y. Yue, G. Eres, X. Wang, and L. Guo, Characterization of Thermal Transport in Micro/Nanoscale Wires by Steady-State Electro-Raman-Thermal Technique, *Applied Physics A*, Vol. 97, pp. 19–23, 2009.
191. M. Li and Y. Yue, Raman-Based Steady-State Thermal Characterization of Multiwall Carbon Nanotube Bundle and Buckypaper, *Journal of Nanoscience and Nanotechnology*, Vol. 15, pp. 3004–3010, 2015.
192. Y. Yue, X. Huang, and X. Wang, Thermal Transport in Multiwall Carbon Nanotube Buckypapers, *Physics Letters A*, Vol. 374, pp. 4144–4151, 2010.
193. Y. Yue, K. Liu, M. Li, and X. Hu, Thermal Manipulation of Carbon Nanotube Fiber by Mechanical Stretching, *Carbon*, Vol. 77, pp. 973–979, 2014.
194. A. Henry, G. Chen, S.J. Plimpton, and A. Thompson, 1D-to-3D Transition of Phonon Heat Conduction in Polyethylene Using Molecular Dynamics Simulations, *Physical Review B*, Vol. 82, pp. 144308, 2010.
195. B.-Y. Cao, Y.-W. Li, J. Kong, H. Chen, Y. Xu, K.-L. Yung, and A. Cai, High Thermal Conductivity of Polyethylene Nanowire Arrays Fabricated by an Improved Nanoporous Template Wetting Technique, *Polymer*, Vol. 52, pp. 1711–1715, 2011.
196. Q. Liao, Z. Liu, W. Liu, C. Deng, and N. Yang, Extremely High Thermal Conductivity of Aligned Carbon Nanotube–Polyethylene Composites, *Scientific Reports*, Vol. 5, pp. 16543, 2015.
197. X. Yu, C. Deng, X. Huang, and N. Yang, Enhancing Thermal Conductivity of Bulk Polyethylene along Two Directions by Paved Crosswise Laminate, *arXiv:1605.01540 [cond-mat]*, 2016.
198. M.T. Pettes, H. Ji, R.S. Ruoff, and L. Shi, Thermal Transport in Three-Dimensional Foam Architectures of Few-Layer Graphene and Ultrathin Graphite, *Nano Letters*, Vol. 12, pp. 2959–2964, 2012.
199. H. Lin, S. Xu, X. Wang, and N. Mei, Significantly Reduced Thermal Diffusivity of Free-Standing Two-Layer Graphene in Graphene Foam, *Nanotechnology*, Vol. 24, pp. 415706, 2013.
200. M. Li, Y. Sun, H. Xiao, X. Hu, and Y. Yue, High Temperature Dependence of Thermal Transport in Graphene Foam, *Nanotechnology*, Vol. 26, pp. 105703, 2015.
201. G. Xin, T. Yao, H. Sun, S.M. Scott, D. Shao, G. Wang, and J. Lian, Highly Thermally Conductive and Mechanically Strong Graphene Fibers, *Science*, Vol. 349, pp. 1083–1087, 2015.
202. Z. Fan, A. Marconnet, S.T. Nguyen, C.Y.H. Lim, and H.M. Duong, Effects of Heat Treatment on the Thermal Properties of Highly Nanoporous Graphene Aerogels Using the Infrared Microscopy Technique, *International Journal of Heat and Mass Transfer*, Vol. 76, pp. 122–127, 2014.
203. M.T. Pettes, M.M. Sadeghi, H. Ji, I. Jo, W. Wu, R.S. Ruoff, and L. Shi, Scattering of Phonons by High-Concentration Isotopic Impurities in Ultrathin Graphite, *Physical Review B*, Vol. 91, pp. 35429, 2015.

204. Y. Xie, Z. Xu, S. Xu, Z. Cheng, N. Hashemi, C. Deng, and X. Wang, The Defect Level and Ideal Thermal Conductivity of Graphene Uncovered by Residual Thermal Reffusivity at the 0 K Limit, *Nanoscale*, Vol. 7, pp. 10101–10110, 2015.

205. J. Ma, Y. Ni, S. Volz, and T. Dumitrică, Thermal Transport in Single-Walled Carbon Nanotubes under Pure Bending, *Physical Review Applied*, Vol. 3, pp. 24014, 2015.

206. Q. Song, M. An, X. Chen, Z. Peng, J. Zang, and N. Yang, Adjustable Thermal Resistor by Reversibly Folding a Graphene Sheet, *Nanoscale*, Vol. 8, pp. 14943–14949, 2016.

207. J.-W. Jiang, N. Yang, B.-S. Wang, and T. Rabczuk, Modulation of Thermal Conductivity in Kinked Silicon Nanowires: Phonon Interchanging and Pinching Effects, *Nano Letters*, Vol. 13, pp. 1670–1674, 2013.

208. A.N. Volkov, T. Shiga, D. Nicholson, J. Shiomi, and L.V. Zhigilei, Effect of Bending Buckling of Carbon Nanotubes on Thermal Conductivity of Carbon Nanotube Materials, *Journal of Applied Physics*, Vol. 111, pp. 53501, 2012.

209. B. Tian, P. Xie, T.J. Kempa, D.C. Bell, and C.M. Lieber, Single-Crystalline Kinked Semiconductor Nanowire Superstructures, *Nature Nanotechnology*, Vol. 4, pp. 824–829, 2009.

210. G. Shen, B. Liang, X. Wang, P.-C. Chen, and C. Zhou, Indium Oxide Nanospirals Made of Kinked Nanowires, *ACS Nano*, Vol. 5, pp. 2155–2161, 2011.

211. J.H. Kim, S.R. Moon, Y. Kim, Z.G. Chen, J. Zou, D.Y. Choi, H.J. Joyce, Q. Gao, H.H. Tan, and C. Jagadish, Taper-Free and Kinked Germanium Nanowires Grown on Silicon via Purging and the Two-Temperature Process, *Nanotechnology*, Vol. 23, pp. 115603, 2012.

212. S.A. Dayeh, J. Wang, N. Li, J.Y. Huang, A.V. Gin, and S.T. Picraux, Growth, Defect Formation, and Morphology Control of Germanium–Silicon Semiconductor Nanowire Heterostructures, *Nano Letters*, Vol. 11, pp. 4200–4206, 2011.

213. S. Li, X. Zhang, L. Zhang, and M. Gao, Twinning-Induced Kinking of Sb-Doped ZnO Nanowires, *Nanotechnology*, Vol. 21, pp. 435602, 2010.

214. D. Ma, H. Ding, H. Meng, L. Feng, Y. Wu, J. Shiomi, and N. Yang, Nano-Cross-Junction Effect on Phonon Transport in Silicon Nanowire Cages, *Physical Review B*, Vol. 94, pp. 165434, 2016.

215. T. Ouyang, Y. Chen, Y. Xie, G.M. Stocks, and J. Zhong, Thermal Conductance Modulator Based on Folded Graphene Nanoribbons, *Applied Physics Letters*, Vol. 99, pp. 233101, 2011.

216. Z. Ni, Y. Wang, T. Yu, Y. You, and Z. Shen, Reduction of Fermi Velocity in Folded Graphene Observed by Resonance Raman Spectroscopy, *Physical Review B*, Vol. 77, pp. 235403, 2008.

217. K. Kim, Z. Lee, B.D. Malone, K.T. Chan, B. Alemán, W. Regan, W. Gannett, M.F. Crommie, M.L. Cohen, and A. Zettl, Multiply Folded Graphene, *Physical Review B*, Vol. 83, pp. 245433, 2011.

218. J. Feng, L. Qi, J.Y. Huang, and J. Li, Geometric and Electronic Structure of Graphene Bilayer Edges, *Physical Review B*, Vol. 80, pp. 165407, 2009.

219. N. Yang, X. Ni, J.-W. Jiang, and B. Li, How Does Folding Modulate Thermal Conductivity of Graphene? *Applied Physics Letters*, Vol. 100, pp. 93107, 2012.

220. D. Li, B. Li, M. Luo, C. Feng, T. Ouyang, and F. Gao, Thermal Transport Properties of Rolled Graphene Nanoribbons, *Applied Physics Letters*, Vol. 103, pp. 71908, 2013.

221. H. Zhang, T. Zhou, G. Xie, J. Cao, and Z. Yang, Thermal Transport in Folded Zigzag and Armchair Graphene Nanoribbons, *Applied Physics Letters*, Vol. 104, pp. 241908, 2014.